

# Topology of Classical Molecular Optimal Control Landscapes for Multi-Target Objectives

Carlee Joe-Wong

*Program in Applied and Computational Mathematics,  
Princeton University, Princeton, NJ, USA*

Tak-San Ho and Herschel Rabitz\*

*Department of Chemistry, Princeton University, Princeton, NJ, USA*

Rebing Wu

*Department of Automation, Tsinghua University, Beijing, P.R. China*

## Abstract

This paper considers laser-driven optimal control of an ensemble of non-interacting molecules whose dynamics lie in classical phase space. The molecules evolve independently under control to distinct final states. We consider a control landscape defined in terms of multi-target (MT) molecular states and analyze the landscape as a functional of the control field. The topology of the MT control landscape is assessed through its gradient and Hessian with respect to the control. Under particular assumptions, the MT control landscape is found to be free of traps that could hinder reaching the objective. The Hessian associated with an optimal control field is shown to have finite rank, indicating an inherent degree of robustness to control noise. Both the absence of traps and rank of the Hessian are shown to be *analogous* to the situation of specifying multiple targets for an ensemble of quantum states. Numerical simulations are presented to illustrate the classical landscape principles and further characterize the system behavior as the control field is optimized.

---

\* hrabitz@princeton.edu

## I. INTRODUCTION

Optimal control of molecular dynamics phenomena with tailored laser pulses is generally expressed in a quantum mechanical context [1–3]. However, classical mechanics often reliably describes nuclear rotational and vibrational motion, especially that of large polyatomic molecules [4–6], including biomolecules [7]. Classical molecular models are therefore often relevant for control of the dynamics on the ground state potential surface. Previous optimal control work suggests that, in some cases, the classical and quantum dynamical models should give qualitatively similar results [8–13]. The conceptual and computational advantage of classically modeled molecular control thus warrants further analysis of the foundations of the subject. Studies considering classically and quantum mechanically modeled molecular control often present suitable algorithms to compute control fields [14–24], and a recent work [25] examined the control landscape of steering a classical system from an initial point in phase space to a final target point. The present paper generalizes the latter findings by considering a finite ensemble of points in phase space (e.g., either corresponding to a discretized set of distinct conditions for a single molecule or to a set of molecules). Control of multiple classical systems has come up in various engineering contexts as well, and the landscape analysis in the present paper could have relevance in that domain [26–29].

An understanding of optimal control may be obtained from analysis of the underlying control landscape, defined as the target objective as a functional of the control field. It is particularly important to assess whether traps, or local extrema with suboptimal landscape values, exist, as their presence could hinder or prevent the search for optimal control fields. Traps would correspond to *critical points* of the landscape, defined as points at which the functional derivative of the objective with respect to the control is zero and the landscape is not at the absolute maximal or minimal value, while the second derivative of the objective (i.e., the Hessian) is respectively negative- or positive-semidefinite. Analysis and simulations in a broad range of closed quantum systems show no evidence of traps upon satisfaction of three specific assumptions: (1) controllability, (2) surjectivity, and (3) free access to control resources [30–34]. Experiments have also verified this conclusion [35, 36]. While violation of one or another of the assumptions can lead to traps, the preponderance of evidence shows

that it is easy to satisfy the assumptions at least to a practical degree [37–39]. Furthermore, a recent paper [40] shows that traps do not exist in the optimal control landscape of open classical and quantum systems, assuming that any desired distribution of final states is reachable; another work [25] reveals that under reasonable assumptions, traps do not exist when a single classical state is sent to a single target state in phase space in a closed system. The present paper builds on these findings by considering optimal control landscapes of multi-target (MT) trajectories starting with an ensemble of distinct initial states in a closed classical phase space that evolve under a control field aiming to reach specified final states.

Quantum mechanical landscape analyses often consider an  $N$ -level closed system with the goal of maximizing the expectation value of a physical observable with the dynamics described by a density matrix. In this study, we consider the classical mechanical *analogue* of quantum mechanically maximizing the MT transition probability that an ensemble of initial quantum states each achieves a specified target [41, 42]. In particular, we specify a final target for each controlled trajectory of a classical ensemble represented by the phase space distribution function. We will compare the classical critical point and Hessian expressions to those in the analogous quantum case. Drawing a control analogy between a quantum ensemble with a finite number of distinct states and a classical ensemble with a finite number of distinct points in phase space is unusual, but informative since they share mathematically similar landscape topologies.

The control of classical systems can sometimes be difficult due to the potential for chaotic behavior, where high sensitivity to initial conditions and control perturbations can present significant numerical issues for finding an optimally controlled trajectory. However, these computational challenges do not pose a *theoretical* barrier to finding an optimal control and examining its (local) stability properties. In addition, some nominally chaotic systems have been shown to exhibit non-chaotic behavior under control [11, 16, 43]; one can also use closed-loop feedback control to stabilize a chaotic system [44–47]. In this work, we consider an open-loop search for an optimal control and assess its stability *post-facto*. A full exploration of the chaotic dynamical regime, however, merits additional attention and is beyond the scope of this work.

Section II describes the ensemble dynamics in the presence of a control field in classical

phase space. We then formulate the classical MT control landscape and use the ensemble dynamics to characterize the critical points of the control landscape in Section III. For comparison, Section IV analyzes the properties of the quantum MT control landscape in an analogous quantum phase space. Section V shows several simulations supporting our theoretical findings about classical control landscapes for various models of molecular ensembles, and Section VI concludes the paper.

## II. FORMULATION OF CONTROLLED CLASSICAL MOLECULAR ENSEMBLES

Consider a classically described molecule of  $n$  atoms, driven by a linearly polarized electric control field  $\epsilon(t)$ . The state of the system at any time  $t$  is specified by the variables  $\mathbf{p} = \mathbf{p}(t)$  and  $\mathbf{q} = \mathbf{q}(t)$ , which are, respectively, the  $3n$ -dimensional momentum and position vectors in a  $6n$ -dimensional phase space  $\Omega$ . We consider an ensemble of chemically identical, non-interacting molecules, whose state trajectories are distributed throughout the phase space. We will write each trajectory as  $\mathbf{z}_\zeta(t) = (\mathbf{q}_\zeta(t), \mathbf{p}_\zeta(t))$  with a distinct initial state  $\zeta$ , i.e.,  $\zeta = (\mathbf{q}(0), \mathbf{p}(0))$ , which evolves independently to a state  $(\mathbf{q}_\zeta(t), \mathbf{p}_\zeta(t))$  at time  $t$ , but under the same control field, based on the Hamiltonian dynamics described below. Though we formulate the optimal control problem for a general initial distribution  $\rho(\zeta, 0)$ , later in Section III B we take  $\rho$  to be a sum of  $\delta$  functions, corresponding to an ensemble of finitely many trajectories. Thus, the ensemble of states  $\mathbf{z}_\zeta(t)$  at each time  $t$  evolves from  $t = 0$  according to Liouville's equation. For simplicity, the explicit time-dependence generally will be dropped with the understanding that  $(\mathbf{q}_\zeta(t), \mathbf{p}_\zeta(t)) \equiv (\mathbf{q}_\zeta, \mathbf{p}_\zeta)$ .

The Hamiltonian  $H(\mathbf{p}_\zeta, \mathbf{q}_\zeta, t)$  of the  $n$ -atom molecule with given initial state  $\zeta$  (i.e., corresponding to one trajectory in the ensemble) can be written as

$$H(\mathbf{p}_\zeta, \mathbf{q}_\zeta, t) = H_0(\mathbf{p}_\zeta, \mathbf{q}_\zeta, t) + H_1(\mathbf{p}_\zeta, \mathbf{q}_\zeta, t), \quad (1)$$

where the field-free and field-molecule interaction Hamiltonians are respectively

$$H_0(\mathbf{p}_\zeta, \mathbf{q}_\zeta, t) = \frac{1}{2} \mathbf{p}_\zeta^T \mathbf{M}^{-1} \mathbf{p}_\zeta + V(\mathbf{q}_\zeta) \quad (2)$$

$$H_1(\mathbf{p}_\zeta, \mathbf{q}_\zeta, t) = -D(\mathbf{q}_\zeta) \epsilon(t). \quad (3)$$

Here we define

$$\mathbf{M} = \begin{bmatrix} \mathbf{m}_1 & 0 & \dots & 0 \\ 0 & \mathbf{m}_2 & \dots & 0 \\ \vdots & \vdots & \ddots & \vdots \\ 0 & 0 & \dots & \mathbf{m}_n \end{bmatrix}, \quad (4)$$

a  $3n \times 3n$  square diagonal matrix composed of  $3 \times 3$  sub-blocks

$$\mathbf{m}_i = \begin{bmatrix} m_i & 0 & 0 \\ 0 & m_i & 0 \\ 0 & 0 & m_i \end{bmatrix}; \quad i = 1, 2, \dots, n, \quad (5)$$

with  $m_i$  being the mass of the  $i$ -th atom. For ease of notation, we set  $\mathcal{N} = 3n$  in the following treatment. The function  $V(\mathbf{q}_\zeta)$  is the potential energy between the atoms. We introduce the square-integrable control field  $\epsilon(t)$ , acting over the time domain  $[0, T]$ , which couples into the Hamiltonian dynamics via  $D(\mathbf{q}_\zeta)$ , the projection of the dipole moment along the linearly polarized control field  $\epsilon(t)$ .

We assume that  $\rho$  falls to zero sufficiently rapidly at infinite distance so that the products of  $\rho(\zeta)$  with  $V(\mathbf{q}_\zeta)$ ,  $D(\mathbf{q}_\zeta)$ ,  $\partial V/\partial \mathbf{q}_\zeta$ , and  $\partial D/\partial \mathbf{q}_\zeta$  are all square-integrable with respect to  $\zeta$  over the phase space. Moreover,  $V(\mathbf{q}_\zeta)$  and  $D(\mathbf{q}_\zeta)$  are considered to be twice differentiable functions of the variable  $\mathbf{q}_\zeta$ . Each molecule in the ensemble is described by the same Hamiltonian governing its dynamics with the same field  $\epsilon(t)$ . The generalization to ensembles of distinct molecules is straightforward; we show numerical examples of this case in Section VD.

To facilitate the derivations, the dynamics of each member of the ensemble is described

by the column vector

$$\mathbf{z}_\zeta(t) = \begin{bmatrix} \mathbf{q}_\zeta(t) \\ \mathbf{p}_\zeta(t) \end{bmatrix}$$

specifying the state at time  $t$  of the trajectory with initial condition  $\mathbf{z}_\zeta(0) \equiv \zeta$  in the corresponding  $2\mathcal{N}$ -dimensional phase space. The evolution of the system for each initial state  $\zeta$  is then governed by Hamilton's equations:

$$\dot{\mathbf{z}}_\zeta = \begin{bmatrix} \dot{\mathbf{q}}_\zeta \\ \dot{\mathbf{p}}_\zeta \end{bmatrix} = \begin{bmatrix} \left( \frac{\partial H(\mathbf{p}_\zeta, \mathbf{q}_\zeta, t)}{\partial \mathbf{p}_\zeta} \right)^T \\ - \left( \frac{\partial H(\mathbf{p}_\zeta, \mathbf{q}_\zeta, t)}{\partial \mathbf{q}_\zeta} \right)^T \end{bmatrix} = K_{\mathcal{N}} \left[ \frac{\partial H(\mathbf{p}_\zeta, \mathbf{q}_\zeta, t)}{\partial \mathbf{q}_\zeta} \quad \frac{\partial H(\mathbf{p}_\zeta, \mathbf{q}_\zeta, t)}{\partial \mathbf{p}_\zeta} \right]^T, \quad (6)$$

where the dot denotes the time derivative and we define

$$K_{\mathcal{N}} = \begin{bmatrix} \emptyset_{\mathcal{N}} & I_{\mathcal{N}} \\ -I_{\mathcal{N}} & \emptyset_{\mathcal{N}} \end{bmatrix}, \quad (7)$$

with  $\emptyset_{\mathcal{N}}$  being the  $\mathcal{N} \times \mathcal{N}$  matrix of zeros and  $I_{\mathcal{N}}$  being the  $\mathcal{N}$ -dimensional identity matrix. The differentiability and integrability assumptions on  $V(\mathbf{q}_\zeta)$ ,  $D(\mathbf{q}_\zeta)$  and  $\epsilon(t)$  imply that Eq. (6) possesses a unique solution [48], given  $\zeta$ . We can rewrite the dynamical equation (6) using the *Poisson bracket*, which is defined as follows:

$$\{f(\mathbf{z}_\zeta(t)), g(\mathbf{z}_\zeta(t))\} \equiv \frac{\partial f}{\partial \mathbf{z}_\zeta(t)} K_{\mathcal{N}} \left( \frac{\partial g}{\partial \mathbf{z}_\zeta(t)} \right)^T. \quad (8)$$

Using the Poisson bracket, Eq. (6) becomes

$$\dot{\mathbf{z}}_\zeta = \{\mathbf{z}_\zeta(t), H(\mathbf{z}_\zeta(t))\} = \{\mathbf{z}_\zeta(t), H_0(\mathbf{z}_\zeta(t))\} + \{\mathbf{z}_\zeta(t), H_1(\mathbf{z}_\zeta(t))\}. \quad (9)$$

### III. CLASSICAL MULTI-TARGET CONTROL LANDSCAPE FOR AN ENSEMBLE OF NON-INTERACTING MOLECULES

This section considers the landscape associated with controlling an ensemble. We will establish the control objective, landscape critical points, and corresponding Hessian expres-

sions for a finite number of ensemble members, which form the basis of the numerical test simulations in Section V. The implications of the findings for the robustness and multiplicity of optimal control solutions will also be discussed. The conclusions drawn about classical control landscape topology rest on a few key assumptions described below; while the satisfaction of these assumptions in any particular application is difficult to assess, the success of the numerical simulations in Section V supports their validity.

### A. Continuous ensemble under control

Consideration of a continuous ensemble is presented for generality and as a basis for consideration in Section III B of the practical scenario of operating with a discrete, finite number of systems (trajectories) under control in phase space. The objective is to control the ensemble, and we consider a quadratic objective function

$$O_\zeta(\mathbf{z}_\zeta(T)) = \frac{1}{2} (\mathbf{z}_\zeta(T) - \mathbf{z}_\zeta^{\text{tar}})^T L_\zeta (\mathbf{z}_\zeta(T) - \mathbf{z}_\zeta^{\text{tar}}) \quad (10)$$

for each initial state  $\zeta$ , where  $L_\zeta$  is a symmetric negative-semidefinite matrix such that  $O_\zeta(\mathbf{z}_\zeta(T)) \leq 0$ . The function  $O_\zeta(\mathbf{z}_\zeta(T))$  is evidently maximized when the associated trajectory at time  $T$  achieves its target state  $\mathbf{z}_\zeta^{\text{tar}}$ . The corresponding MT control landscape  $J[\epsilon(t)]$  as a function of the control field  $\epsilon(t)$  may be defined as an average of the objective  $O_\zeta$  over the phase space distribution of initial states  $\rho(\zeta, 0)$ :

$$J[\epsilon(t)] = \int_{\Omega} O_\zeta(\mathbf{z}_\zeta(T)) \rho(\zeta, 0) d\zeta, \quad (11)$$

where the optimization goal is to achieve  $\max_{\epsilon(t)} J[\epsilon(t)]$ .

It is possible to include other terms in the objective functional  $J$  (e.g.,  $J \equiv \int_{\Omega} O_\zeta(\mathbf{z}_\zeta(T)) \rho(\zeta, 0) d\zeta + \alpha \int_0^T \epsilon(t)^2 dt$ ,  $\alpha < 0$ ) to bias the class of controls, but in this work we focus on the fundamental case where  $J[\epsilon(t)]$  is given in Eq. (11) to assess the landscape topology without further terms in the objective functional or constraints on the field.

Critical points of the MT control landscape  $J[\epsilon(t)]$  correspond to the zero gradient con-

dition

$$\frac{\delta J}{\delta \epsilon(t)} = \int_{\Omega} \frac{\partial O_{\zeta}}{\partial \mathbf{z}_{\zeta}(T)} \frac{\delta \mathbf{z}_{\zeta}(T)}{\delta \epsilon(t)} \rho(\zeta, 0) d\zeta = 0, \quad t \in [0, T], \quad (12)$$

where  $\partial O_{\zeta}/\partial \mathbf{z}_{\zeta}(T) = [\mathbf{z}_{\zeta}(T) - \mathbf{z}_{\zeta}^{\text{tar}}]^T L_{\zeta}$  and an explicit expression for the functional derivative  $\delta \mathbf{z}_{\zeta}(T)/\delta \epsilon(t)$  can be readily derived using the Poisson bracket formulation for the system dynamics in Eq. (9). Specifically, consider a perturbation of the control  $\epsilon(t) \rightarrow \epsilon(t) + \delta \epsilon(t)$  in Eq. (6) [49], with  $\delta \mathbf{z}_{\zeta}(t)$  denoting the response in  $\mathbf{z}_{\zeta}(t)$ . From Eq. (9), we see that the first order variation for each trajectory is

$$\delta \dot{\mathbf{z}}_{\zeta}(t) = A_{\zeta}(t) \delta \mathbf{z}_{\zeta}(t) + B_{\zeta}(t) \delta \epsilon(t), \quad (13)$$

where  $\delta \mathbf{z}_{\zeta}(t) = [\delta \mathbf{q}_{\zeta}^T(t) \quad \delta \mathbf{p}_{\zeta}^T(t)]^T$ , the  $2\mathcal{N} \times 2\mathcal{N}$  matrix  $A_{\zeta}(t) = K_{\mathcal{N}}(\partial^2 H/\partial \mathbf{z}_{\zeta}(t)^2)$ , and the  $2\mathcal{N} \times 1$  vector  $B_{\zeta}(t) = K_{\mathcal{N}}(\partial H_1/\partial \mathbf{z}_{\zeta}(t))^T = -K_{\mathcal{N}}(\partial D/\partial \mathbf{z}_{\zeta}(t))^T \epsilon(t)$ . Integrating Eq. (13) yields [50]

$$\delta \mathbf{z}_{\zeta}(T) = M_{\zeta}(T) \int_0^T M_{\zeta}^{-1}(t) B_{\zeta}(t) \delta \epsilon(t) dt, \quad \dot{M}_{\zeta}(t) = A_{\zeta}(t) M_{\zeta}(t), \quad M_{\zeta}(0) = I_{2\mathcal{N}}. \quad (14)$$

Here  $M_{\zeta}(t)$  is the so-called fundamental matrix  $M_{\zeta}(t) = \partial \mathbf{z}_{\zeta}(t)/\partial \mathbf{z}_{\zeta}(0)$ , with the  $(i, j)$  entry of  $M_{\zeta}(t)$  being  $\partial z_{\zeta,i}(t)/\partial z_{\zeta,j}(0)$ , representing the sensitivity of the  $i$ th component of the state at time  $t$  to the  $j$ th component of the state at the initial time. The matrix  $M_{\zeta}(t)$  is also symplectic [51] and thus invertible. We define  $M_{\zeta}(t, t') = M_{\zeta}(t) M_{\zeta}^{-1}(t')$  and use Eq. (14) to derive

$$\frac{\delta \mathbf{z}_{\zeta}(T)}{\delta \epsilon(t)} = M_{\zeta}(T, t) B_{\zeta}(t) = \frac{\partial \mathbf{z}_{\zeta}(T)}{\partial \zeta} \frac{\partial \zeta}{\partial \mathbf{z}_{\zeta}(t)} K_{\mathcal{N}} \left( \frac{\partial H_1}{\partial \mathbf{z}_{\zeta}(t)} \right)^T = \frac{\partial \mathbf{z}_{\zeta}(T)}{\partial \mathbf{z}_{\zeta}(t)} K_{\mathcal{N}} \left( \frac{\partial H_1}{\partial \mathbf{z}_{\zeta}(t)} \right)^T. \quad (15)$$

Here  $\delta \mathbf{z}_{\zeta}(T)/\delta \epsilon(t)$  is the functional derivative  $\delta \epsilon(t) \rightarrow \delta \mathbf{z}_{\zeta}(T)$  of the end-point mappings  $\epsilon \rightarrow \mathbf{z}_{\zeta}(T)$ , defined in the neighborhood of the control field  $\epsilon(t)$ . The behavior of this end-point mapping is important for achieving optimal control, as explained in Section III B.

Obtaining control over a continuous ensemble is very demanding, as nominally each differential variation  $\zeta + \delta \zeta$  of a state  $\zeta$  needs to be separately controlled. In practice, numerical calculations are always carried out upon a discrete set of initial points in phase space, and

molecules are inherently discrete objects. In this sense, control over the full distribution needs to be understood to an acceptable degree of resolution; the remainder of the paper therefore takes a practical discrete perspective.

## B. Finite ensemble under control

In practical circumstances, control simulations will treat either (i) a finite set of molecules with each starting at a separate point in phase space, or (ii) a discretized distribution of a single molecule expressed as a finitely resolved picture of the density over phase space under control. Both cases can be expressed in terms of a finite number of  $\mathcal{M}$  trajectories. Equation (11) then becomes

$$J = \sum_{j=1}^{\mathcal{M}} \rho_j O_j(\mathbf{z}_j(T)), \quad (16)$$

where  $j$  is used instead of  $\zeta$  to index the trajectories,  $\rho_j > 0$  is the initial distribution weight of the  $j$ th trajectory, and  $O_j$  is the discrete form of the target function set out in Eq. (10), i.e.,  $O_j(\mathbf{z}_j(T)) = (1/2) [\mathbf{z}_j(T) - \mathbf{z}_j^{\text{tar}}]^T L_j [\mathbf{z}_j(T) - \mathbf{z}_j^{\text{tar}}]$ . We can formally view the transition from Eq. (11) to Eq. (16) as arising from the original initial distribution,  $\rho(\zeta, 0)$ , reduced to a sum of  $\mathcal{M}$  phase space  $\delta$  functions, with each generating a unique trajectory under application of the control field. We use  $O_j$  to denote the objective function for the  $j$ th trajectory.

We assume that the collective system is controllable, denoting this as Assumption 1, in that with an appropriate control  $\epsilon$  any collection of distinct initial states  $\{\mathbf{z}_j(0)\}$  can be steered to any associated set of distinct target states  $\{\mathbf{z}_j^{\text{tar}}\}$  at some time  $T$  (i.e.,  $\mathbf{z}_j(T) = \mathbf{z}_j^{\text{tar}}$  for  $i = 1, 2, \dots, \mathcal{M}$ ). While controllability becomes a stronger demand as we take the limit to an ever denser ensemble of initial or target states, it is a reasonable assumption for the finite ensembles considered here. As we show in the discussion below, however, controllability alone is not sufficient to ensure the absence of traps in the landscape. In particular, while controllability guarantees that there exists a control field that will steer the initial state to the target state at time  $T$ , it does not guarantee that a myopic gradient algorithm can find the optimal field. We make two additional assumptions in the discussion below to ensure

that an optimal field can be found. These are analogues of conditions known to be sufficient to establish a trap-free landscape in quantum control [30].

### 1. Landscape critical points

The first step in assessing the landscape topology consists of locating critical points where  $\delta J/\delta\epsilon(t) = 0$ ,  $t \in [0, T]$ . Taking the derivative of Eq. (16), we find that

$$\frac{\delta J}{\delta\epsilon(t)} = \sum_{j=1}^{\mathcal{M}} \rho_j \frac{\partial O_j(\mathbf{z}_j(T))}{\partial \mathbf{z}_j(T)} \frac{\delta \mathbf{z}_j(T)}{\delta\epsilon(t)} = \sum_{j=1}^{\mathcal{M}} \rho_j \left[ \mathbf{z}_j(T) - \mathbf{z}_j^{\text{tar}} \right]^T L_j \frac{\delta \mathbf{z}_j(T)}{\delta\epsilon(t)}. \quad (17)$$

We may rewrite this expression as a scalar product by concatenating the column vectors  $\mathbf{z}_j$  into one large,  $2\mathcal{M}\mathcal{N}$ -dimensional column vector  $\mathbf{Z}$ :

$$\frac{\delta J}{\delta\epsilon(t)} = \frac{\partial J}{\partial \mathbf{Z}(T)} \frac{\delta \mathbf{Z}(T)}{\delta\epsilon(t)}, \quad (18)$$

where  $\partial J/\partial \mathbf{Z}(T)$  is a  $2\mathcal{M}\mathcal{N}$ -dimensional row vector, i.e.,

$$\begin{aligned} \frac{\partial J}{\partial \mathbf{Z}(T)} &= \left[ \rho_1 \frac{\partial O_1}{\partial \mathbf{z}_1(T)} \quad \rho_2 \frac{\partial O_2}{\partial \mathbf{z}_2(T)} \quad \cdots \quad \rho_{\mathcal{M}} \frac{\partial O_{\mathcal{M}}}{\partial \mathbf{z}_{\mathcal{M}}(T)} \right] \\ &= \left[ \rho_1 (\mathbf{z}_1(T) - \mathbf{z}_1^{\text{tar}})^T L_1, \quad \rho_2 (\mathbf{z}_2(T) - \mathbf{z}_2^{\text{tar}})^T L_2, \quad \dots, \quad \rho_{\mathcal{M}} (\mathbf{z}_{\mathcal{M}}(T) - \mathbf{z}_{\mathcal{M}}^{\text{tar}})^T L_{\mathcal{M}} \right], \end{aligned} \quad (19)$$

and  $\delta \mathbf{Z}(T)/\delta\epsilon(t)$  is a  $2\mathcal{M}\mathcal{N}$ -dimensional column vector, i.e.,

$$\frac{\delta \mathbf{Z}(T)}{\delta\epsilon(t)} = \begin{bmatrix} \delta \mathbf{z}_1(T)/\delta\epsilon(t) \\ \delta \mathbf{z}_2(T)/\delta\epsilon(t) \\ \vdots \\ \delta \mathbf{z}_{\mathcal{M}}(T)/\delta\epsilon(t) \end{bmatrix}. \quad (20)$$

It is readily seen that if  $\{\delta \mathbf{Z}(T)/\delta\epsilon(t)\}$  spans  $\mathbb{R}^{2\mathcal{M}\mathcal{N}}$ , then  $\delta J/\delta\epsilon(\cdot) = 0$  in Eq. (18) implies

that  $\partial J/\partial \mathbf{Z}(T) = 0$ , leading to the kinematic critical conditions

$$\frac{\partial O_j}{\partial \mathbf{z}_j(T)} = (\mathbf{z}_j(T) - \mathbf{z}_j^{\text{tar}})^T L_j = 0 \quad \forall j = 1, 2, \dots, \mathcal{M}, \quad (21)$$

where we use the fact that  $\rho_j > 0 \forall j$ . Satisfaction of Eq. (21) is the defining criterion of a *kinematic critical point*. Thus, all critical points (i.e., control fields  $\epsilon(t)$  with  $\delta J/\delta \epsilon = 0$ ) are kinematic if  $\{\delta \mathbf{Z}(T)/\delta \epsilon(t)\}$  spans  $\mathbb{R}^{2\mathcal{M}\mathcal{N}}$ , or equivalently if the family of linear functionals  $\{\delta \mathbf{Z}(T)/\delta \epsilon(t), t \in [0, T]\}$  is *surjective* on  $\mathbb{R}^{2\mathcal{M}\mathcal{N}}$ , which we take as our Assumption 2. It is likely that this assumption will be satisfied to a practical degree, as the dynamics in Eq. (14) for each  $M_j(t)$  depend on time in a complicated manner, via  $\mathbf{q}_j(t)$ ,  $\mathbf{p}_j(t)$ , and  $\epsilon(t)$ , and the dynamical equation (6) has a unique and distinct solution for each initial state. An ensemble with a set of  $\mathcal{M}$  distinct molecules and corresponding Hamiltonians  $\{H_j\}$  makes surjectivity of  $\{\delta \mathbf{Z}(T)/\delta \epsilon(t)\}$  even more likely by introducing additional dynamical richness into the trajectory ensemble (e.g., Section VD presents some examples). We may view satisfaction of surjectivity as assuring that any differential change  $\delta \mathbf{z}(T)$  at an arbitrary location on the landscape has a corresponding differential change in the control  $\delta \epsilon(t)$  that can meet the demand. Thus, satisfaction of surjectivity can be viewed as permitting local freedom to move to any neighboring location, which is important as a sufficient condition for exploiting a local gradient to climb the landscape. Surjectivity is distinct from controllability, which assumes that some control field exists that will produce an optimal solution.

In the landscape analysis we also assume that free access is available to any desired control field  $\epsilon(t)$  resources, which we take as our Assumption 3. This assumption is necessary so as to avoid limiting the practical ability to satisfy Assumptions 1 (controllability) and 2 (surjectivity). In realistic circumstances, control fields available in system-specific physically relevant spectral domain(s) are likely adequate to avoid hindering the dynamics. In addition to the three physical assumptions above, we have also considered that differentiability and integrability of  $\rho$ ,  $V$ , and  $D$  are satisfied.

Taken together, the three assumptions present sufficient conditions whose collective satisfaction allows one to start with any initial field and maximize the objective function, even with a myopic gradient algorithm. Importantly, the three assumptions represent independent

properties. There are many examples of classical systems where controllability is satisfied but surjectivity is not [49]. Examples of controllable but non-surjective systems can also be found in the quantum control literature [39], where this situation may, or may not, lead to landscape traps [52] depending on the circumstances.

Surjectivity (Assumption 2) is perhaps the most subtle of the assumptions to assess *a priori*, and its satisfaction depends on the dynamics being sufficiently rich; analogous Assumptions to 1, 2, and 3 are made for the control of quantum systems in [30, 53]. We numerically investigate whether surjectivity holds for some sample model systems in Section V; the resultant satisfactory behavior also confirms that the controllability and control resource assumptions are at least adequately satisfied. The assumptions should be viewed as sufficient conditions to assess the landscape topology, and in this regard we also present an example in Section V of an uncontrollable system for which good results are nonetheless still attained.

## 2. Landscape Hessian analysis

After locating the critical points on the landscape  $J[\epsilon(t)]$ , the next step is to determine their local character as either extrema of some type (i.e., global or suboptimal) or intermediate saddle features. Towards this end, we can differentiate the critical point equation Eq. (17) to obtain an expression for the Hessian  $\delta^2 J / \delta \epsilon(t) \delta \epsilon(t')$ , denoted as  $\mathcal{H}(t, t')$ :

$$\mathcal{H}(t, t') = \sum_{j=1}^{\mathcal{M}} \rho_j \left( \left( \frac{\delta \mathbf{z}_j(T)}{\delta \epsilon(t')} \right)^T \frac{\partial^2 O_j}{\partial \mathbf{z}_j(T)^2} \frac{\delta \mathbf{z}_j(T)}{\delta \epsilon(t)} + \frac{\partial O_j}{\partial \mathbf{z}_j(T)} \frac{\delta^2 \mathbf{z}_j(T)}{\delta \epsilon(t') \delta \epsilon(t)} \right). \quad (22)$$

At the kinematic critical points, we have  $\rho_j (\partial O_j / \partial \mathbf{z}_j(T)) = 0$  for each  $j$ , so that

$$\mathcal{H}(t, t') = \sum_{j=1}^{\mathcal{M}} \rho_j \left( \frac{\delta \mathbf{z}_j(T)}{\delta \epsilon(t')} \right)^T \frac{\partial^2 O_j}{\partial \mathbf{z}_j(T)^2} \frac{\delta \mathbf{z}_j(T)}{\delta \epsilon(t)} = \sum_{j=1}^{\mathcal{M}} \rho_j \left( \frac{\delta \mathbf{z}_j(T)}{\delta \epsilon(t')} \right)^T L_j \frac{\delta \mathbf{z}_j(T)}{\delta \epsilon(t)}. \quad (23)$$

Rewriting this equation in matrix form produces

$$\mathcal{H}(t, t') = \left( \frac{\delta \mathbf{Z}(T)}{\delta \epsilon(t')} \right)^T X \frac{\delta \mathbf{Z}(T)}{\delta \epsilon(t)}, \quad (24)$$

where  $X$  is defined as the block diagonal matrix  $X = \text{diag} \{ \rho_1 L_1, \rho_2 L_2, \dots, \rho_M L_M \}$ . We can now easily see that the signature of the Hessian in Eq. (24) is exactly the signature of  $X$  at the kinematic critical points [32, 54], assuming that  $\delta \mathbf{Z}(T)/\delta \epsilon(t)$  is full rank (i.e., the surjectivity assumption is satisfied). Thus, since the  $L_j$  are negative semi-definite matrices, the Hessian is also negative semi-definite at all critical points. No critical point exists as a trap (i.e., a local, non-global maximum):  $O_j(\mathbf{z}_j(T))$  has its unique maximum value  $O_j(\mathbf{z}_j(T)) = 0$  when the kinematic critical point criterion in Eq. (21) is satisfied. Thus,  $J[\epsilon(t)]$  reaches its maximum value of 0 at all critical points (i.e., corresponding to the set of all controls that produce  $J = 0$ ) of the control landscape, and neither traps nor saddles arise.

The Hessian in Eq. (24) is of finite rank, implying the presence of a null space and an inherent degree of robustness for optimal control field solutions. We can then diagonalize the matrix  $X$  at any given kinematic critical point and rewrite the Hessian as

$$\mathcal{H}(t, t') = \left( \frac{\delta \mathbf{Z}(T)}{\delta \epsilon(t')} \right)^T \mathbf{P}^T \mathbf{\Sigma} \mathbf{P} \frac{\delta \mathbf{Z}(T)}{\delta \epsilon(t)}, \quad (25)$$

where  $\mathbf{P}$  is a  $2\mathcal{M}\mathcal{N}$ -dimensional orthogonal matrix and  $\mathbf{\Sigma}$  is diagonal. Thus, letting  $\phi_l(t)$  denote the  $l$ th entry in the vector  $\mathbf{P}(\delta \mathbf{Z}(T)/\delta \epsilon(t))$ , we have

$$\mathcal{H}(t, t') = \sum_{l=1}^{2\mathcal{M}\mathcal{N}} \sigma_l \phi_l(t) \phi_l(t'), \quad (26)$$

where  $\sigma_l$  is the  $l$ th diagonal entry of  $\mathbf{\Sigma}$ . Equation (26) allows for bounding the second-order variation of  $J[\epsilon(t)]$  about the absolute landscape maximum due to a variation  $\epsilon(t) \rightarrow$

$\epsilon(t) + \delta\epsilon(t)$  in the control:

$$|\delta J| = \frac{1}{2} \sum_{l=1}^{2\mathcal{M}\mathcal{N}} \sigma_l \int_0^T \int_0^T |\phi_l(t)\phi_l(t')\delta\epsilon(t)\delta\epsilon(t')| dt dt' \quad (27)$$

$$\leq \frac{1}{2} \sum_{l=1}^{2\mathcal{M}\mathcal{N}} \sigma_l \left( \int_0^T \phi_l^2(t) dt \right) \times \left( \int_0^T [\delta\epsilon(t)]^2 dt \right) \quad (28)$$

$$\leq T \|\delta\epsilon\|_T^2 \text{Tr } \mathcal{H}, \quad (29)$$

where  $\|\cdot\|_T$  is defined as

$$\|f\|_T^2 = \frac{1}{T} \int_0^T f^T f dt$$

and the trace of the Hessian satisfies

$$\text{Tr } \mathcal{H} = \int_0^T \mathcal{H}(t, t) dt = \sum_{j=1}^{2\mathcal{M}\mathcal{N}} \sigma_j \int_0^T \phi_j^2(t) dt \leq T (\text{Tr } X) \left\| \frac{\delta \mathbf{Z}(T)}{\delta \epsilon(t)} \right\|_T^2. \quad (30)$$

Assuming a uniform bound on  $\delta \mathbf{z}_j(T)/\delta \epsilon(t) = M_j(T, t)B_j(t)$  for all  $j$ , we see from Eq. (29) that the variation in  $J$  due to a variation  $\epsilon(t) \rightarrow \epsilon(t) + \delta\epsilon(t)$  is proportional to the square of the time-averaged norm of  $\delta\epsilon(t)$ , i.e., the energy in the field noise. A bound on the  $\delta \mathbf{z}_j(T)/\delta \epsilon(t)$  is consistent with each entry in  $\partial D_j/\partial \mathbf{z}_j(t)$  and  $M_j(T, t)$  being bounded; this follows from Eq. (14) and the set of molecular trajectories  $\mathbf{z}_j(t)$  being bounded, as they start from a bounded set of initial states  $\mathbf{z}_j(0)$  and both  $T$  and  $\|\epsilon\|_T$  are finite. The bound on the Hessian in Eq. (30) implies an additional degree of robustness to disturbances, resulting from a lack of extremely “steep” paths off the top of the landscape.

#### IV. COMPARISON TO ANALOGOUS QUANTUM MULTI-TARGET CONTROL LANDSCAPES

This section will demonstrate the relationship between the results of Section III and those for an analogous ensemble quantum system. We emphasize that the relationship between the classical and quantum cases is that of an analogy rather than one being the limit of the other scenario. Thus, in analogy to the finite ensemble of classical molecular trajectories in Section

III, we consider a quantum system with  $N$  distinct, linearly independent  $N$ -level quantum pure states, represented by  $|\psi_j(t)\rangle$ ,  $j = 1, 2, \dots, N$ . We specify targets for  $M \leq N$  of these quantum states. The variable  $M$  is thus analogous to the number of classical trajectories,  $\mathcal{M}$ , in Section II, while the number of states  $N$  is analogous to the number of classical atoms  $n$ . The dynamics of each quantum state satisfies the time-dependent Schrödinger equation

$$i\hbar \frac{\partial |\psi_j(t)\rangle}{\partial t} = (H_0^{\text{qu}} - \mu\epsilon(t)) |\psi_j(t)\rangle, \quad (31)$$

where (using standard notations in quantum control)  $H_0^{\text{qu}}$  is the unperturbed Hamiltonian and  $\mu$  is the dipole moment operator. We define the time-dependent Hamiltonian  $H^{\text{qu}}(t)$  as  $H^{\text{qu}}(t) = H_0^{\text{qu}} - \mu\epsilon(t)$  and, for simplicity, we will assume that both  $H_0$  and  $\mu$  are real symmetric matrices. Furthermore, we assume without loss of generality that all initial states  $|\psi_j(0)\rangle$  are linearly independent from each other.

The quantum Hamiltonian dynamics can be written analogously to the classical case [55] if we identify the quantum states  $|\psi_j(t)\rangle$  with the unit vectors

$$\mathbf{x}_j(t) \equiv \frac{1}{\sqrt{2}} \begin{bmatrix} \mathbf{q}_j^{\text{qu}}(t) \\ \mathbf{p}_j^{\text{qu}}(t) \end{bmatrix}, \quad \|\mathbf{x}_j^T(t)\|^2 = \mathbf{x}_j^T(t)\mathbf{x}_j(t) = 1,$$

where  $\mathbf{q}_j^{\text{qu}}(t) \equiv \sqrt{2}\Re(|\psi_j(t)\rangle)$  and  $\mathbf{p}_j^{\text{qu}}(t) \equiv \sqrt{2}\Im(|\psi_j(t)\rangle)$ . These vectors evolve according to Hamiltonian dynamics

$$\begin{aligned} \frac{d\mathbf{q}_j^{\text{qu}}(t)}{dt} &= \nabla_{\mathbf{p}_j^{\text{qu}}} \mathbf{H}_j^{\text{qu}}(\mathbf{q}_j^{\text{qu}}, \mathbf{p}_j^{\text{qu}}, t) = \frac{1}{\hbar} [H_0^{\text{qu}} - \mu\epsilon(t)] \mathbf{p}_j^{\text{qu}}(t), \\ \frac{d\mathbf{p}_j^{\text{qu}}(t)}{dt} &= -\nabla_{\mathbf{q}_j^{\text{qu}}} \mathbf{H}_j^{\text{qu}}(\mathbf{q}_j^{\text{qu}}, \mathbf{p}_j^{\text{qu}}, t) = \frac{-1}{\hbar} [H_0^{\text{qu}} - \mu\epsilon(t)] \mathbf{q}_j^{\text{qu}}(t), \end{aligned} \quad (32)$$

where the Hamiltonian  $\mathbf{H}_j^{\text{qu}}$  is defined as

$$\begin{aligned} \mathbf{H}_j^{\text{qu}} &\equiv \frac{1}{2\hbar} \begin{bmatrix} \mathbf{q}_j^{\text{qu}T}(t) & \mathbf{p}_j^{\text{qu}T}(t) \end{bmatrix} \begin{bmatrix} H_0^{\text{qu}} - \mu\epsilon(t) & 0 \\ 0 & H_0^{\text{qu}} - \mu\epsilon(t) \end{bmatrix} \begin{bmatrix} \mathbf{q}_j^{\text{qu}}(t) \\ \mathbf{p}_j^{\text{qu}}(t) \end{bmatrix} \\ &= \frac{1}{2\hbar} \left( \mathbf{p}_j^{\text{qu},T}(t) [H_0^{\text{qu}} - \mu\epsilon(t)] \mathbf{p}_j^{\text{qu}}(t) + \mathbf{q}_j^{\text{qu},T}(t) [H_0^{\text{qu}} - \mu\epsilon(t)] \mathbf{q}_j^{\text{qu}}(t) \right) \end{aligned}$$

Note that  $\mathbf{H}_j^{\text{qu}}$  is quadratic in  $\mathbf{x}_j(t)$ , which comes from the linearity of the quantum dynamics in Eq. (31). In contrast, the classical Hamiltonian given in Eqs. (1–3) can be arbitrarily nonlinear in the state vector  $\mathbf{z}_\zeta(t)$ .

As in the classical case considered in Sections II and III, we consider unique target states  $\mathbf{x}_j^{\text{tar}}$  for each state  $j$ . To meet these targets, we consider multi-objective functions  $O_j^{\text{qu}}(\mathbf{x}_j(T)) = -(\mathbf{x}_j(T) - \mathbf{x}_j^{\text{tar}})^T (\mathbf{x}_j(T) - \mathbf{x}_j^{\text{tar}}) / 2$  that are maximized subject to the constraints  $\mathbf{x}_j^T(T)\mathbf{x}_j(T) = \langle \psi_j(T) | \psi_j(T) \rangle = 1$ ,  $j = 1, \dots, M$ . We thus define the functional

$$J^{\text{qu}}[\epsilon(t)] = \sum_{j=1}^M r_j O_j^{\text{qu}}(\mathbf{x}_j(T)) \quad (33)$$

as the quantum MT control landscape in the control space specified over the control field  $\epsilon(t)$ , where we normalize the weights  $r_j > 0$  so that  $\sum_{j=1}^M r_j = 1$ . This landscape is similar to that of the so-called ‘‘W problem’’ of generating a specific unitary transformation  $W$  from a given set of initial states to desired final states at time  $T$ , which was considered in [56, 57]. However, our scenario is a special case in that if  $M < N$ , then the  $M$  initial states seek to reach the  $M$  target states, forming an  $N \times M$  portion of the target matrix  $W$ . Importantly, for the quantum control case we adopt the same three Assumptions made in the classical context. Here, Assumption 1 is that any distinct set of  $N$  initial states  $\{|\psi_j(0)\rangle\}$  may be steered to reach any set of distinct final states  $\{|\psi_j(T)\rangle\}$  at time  $T$ . Similarly we adopt the surjectivity Assumption 2 (see the discussion below Eq. (34)) and Assumption 3 that access is available to any desired control field. In the discussion below, we derive critical point and Hessian expressions for this control landscape.

Critical points of  $J^{\text{qu}}$  occur when  $\delta J^{\text{qu}} / \delta \epsilon(t) = 0$ , leading to the relation

$$\sum_{j=1}^M r_j (\mathbf{x}_j(T) - \mathbf{x}_j^{\text{tar}})^T \frac{\delta \mathbf{x}_j(T)}{\delta \epsilon(t)} = 0 \quad \forall t \in [0, T] \quad (34)$$

To follow the classical analysis of such landscape critical points, we now wish to assume that the concatenated vector  $\{\delta \mathbf{x}_j(T) / \delta \epsilon(t)\}$  is surjective, yielding the condition  $\mathbf{x}_j(T) = \mathbf{x}_j^{\text{tar}}$  for each trajectory  $j$  at all critical points. However, in the quantum scenario  $\delta \mathbf{x}_j(T) / \delta \epsilon(t)$  is re-

stricted by the requirement that  $\|\mathbf{x}_j\| = 1$ , imposing the condition that  $\delta(\mathbf{x}_j^T(T)\mathbf{x}_j(T))/\delta\epsilon(t) = 2\mathbf{x}_j^T(T)(\delta\mathbf{x}_j(T)/\delta\epsilon(t)) = 0$ . Thus, each  $\delta\mathbf{x}_j(T)/\delta\epsilon(t)$  is of rank at most  $2N - 1$ , and the concatenated vectors  $\{\delta\mathbf{x}_j(T)/\delta\epsilon(t)\}$  have rank at most  $(2N - 1)M$ . Assuming that they achieve this maximum rank, Eq. (34) is satisfied when

$$\mathbf{x}_j(T) - \mathbf{x}_j^{\text{tar}} = \alpha_j \mathbf{x}_j(T) \quad (35)$$

for a scalar  $\alpha_j \in \mathbb{R}$ . Equivalently,  $\mathbf{x}_j(T) = \mathbf{x}_j^{\text{tar}}/(1 - \alpha_j)$ . Since both  $\mathbf{x}_j(T)$  and  $\mathbf{x}_j^{\text{tar}}$  are unit vectors, we must then have  $1 - \alpha_j = \pm 1$ , or equivalently  $\alpha_j = 0$  or  $2$ , leading to the relation  $\mathbf{x}_j(T) = \pm \mathbf{x}_j^{\text{tar}}$ . As a result, it is seen that  $J^{\text{qu}} = -\sum_{j=1}^M r_j \alpha_j^2$  at the kinematic critical points, which renders a global maximum value equal to 0 and a global minimum value equal to  $-4$ , corresponding to all  $\alpha_j = 0$  and all  $\alpha_j = 2$  respectively.

The nature of these landscape critical points (i.e., whether they correspond to minima, maxima, or saddles) depends on the signature of the quantum Hessian matrix. We can write the Hessian as  $\mathcal{H}^{\text{qu}}(t, t') = \sum_j \mathcal{H}_j^{\text{qu}}(t, t')$  and consider the term  $\mathcal{H}_j^{\text{qu}}(t, t')$  for each trajectory  $j$  by differentiating Eq. (33):

$$\mathcal{H}_j^{\text{qu}}(t, t') = r_j \left( \frac{\delta\mathbf{x}_j^T(T)}{\delta\epsilon(t')} \frac{\partial^2 O_j^{\text{qu}}}{\partial\mathbf{x}_j(T)^2} \frac{\delta\mathbf{x}_j(T)}{\delta\epsilon(t)} + \frac{\partial O_j^{\text{qu}}}{\partial\mathbf{x}_j(T)} \frac{\delta^2\mathbf{x}_j(T)}{\delta\epsilon(t')\delta\epsilon(t)} \right), \quad (36)$$

where  $\partial O_j^{\text{qu}}/\partial\mathbf{x}_j(T) = -[\mathbf{x}_j(T) - \mathbf{x}_j^{\text{tar}}]^T$  and  $\partial^2 O_j^{\text{qu}}/\partial\mathbf{x}_j^2(T) = -I$ . Using Eq. (35), we thus find that

$$\mathcal{H}_j^{\text{qu}}(t, t') = -r_j \left( \frac{\delta\mathbf{x}_j^T(T)}{\delta\epsilon(t')} \frac{\delta\mathbf{x}_j(T)}{\delta\epsilon(t)} + \alpha_j \mathbf{x}_j^T(T) \frac{\delta^2\mathbf{x}_j(T)}{\delta\epsilon(t')\delta\epsilon(t)} \right),$$

where  $\alpha_j = 0$  or  $2$ , corresponding to  $\mathbf{x}_j(T) = \mathbf{x}_j^{\text{tar}}$  and  $\mathbf{x}_j(T) = -\mathbf{x}_j^{\text{tar}}$  respectively. We can further simplify the Hessian in Eq. (36) by noting that the requirement  $\|\mathbf{x}_j(T)\| = 1$  implies that the second derivative satisfies

$$\frac{\delta^2(\mathbf{x}_j^T(T)\mathbf{x}_j(T))}{\delta\epsilon(t')\delta\epsilon(t)} = 2 \frac{\delta\mathbf{x}_j^T(T)}{\delta\epsilon(t')} \frac{\delta\mathbf{x}_j(T)}{\delta\epsilon(t)} + 2\mathbf{x}_j^T(T) \frac{\delta^2\mathbf{x}_j(T)}{\delta\epsilon(t')\delta\epsilon(t)} = 0.$$

Thus, using Eq. (36) we can derive the full Hessian

$$\mathcal{H}^{\text{qu}}(t, t') = - \sum_{j=1}^M r_j (1 - \alpha_j) \left( \frac{\delta \mathbf{x}_j^T(T)}{\delta \epsilon(t')} \frac{\delta \mathbf{x}_j(T)}{\delta \epsilon(t)} \right). \quad (37)$$

The Hessian is therefore a symmetric kernel with a finite number of nonzero eigenvalues, as in the classical case. By defining the functions  $\phi_{j,k}(t)$  as the  $k$ th element of  $\delta \mathbf{x}_j(T)/\delta \epsilon(t)$ , we can write Eq. (37) as a symmetric sum of functions  $\phi_{j,k}$ :

$$\mathcal{H}^{\text{qu}}(t, t') = - \sum_{j=1}^M r_j (1 - \alpha_j) \sum_{k=1}^M \phi_{j,k}(t) \phi_{j,k}(t'). \quad (38)$$

We now observe that the surjectivity assumption that  $\delta \mathbf{x}_j(T)/\delta \epsilon(t)$  has rank  $2N - 1$  implies that  $\mathcal{H}_j^{\text{qu}}$  has rank of at most  $2N - 2$ . Thus, the  $\{\phi_{j,k}\}$  in Eq. (38) can be orthogonalized to a set of at most  $(2N - 2)M$  linear independent, orthogonal functions.

We can now classify critical points into three types depending on the  $\alpha_j$  values for each trajectory and determine the signature of Eq. (38) for each type. In the first type of critical point,  $\alpha_j = 0$  for all trajectories, indicating all trajectories achieve their targets (i.e.,  $\mathbf{x}_j(T) = \mathbf{x}_j^{\text{tar}}$ ) and the Hessian is strictly negative-semidefinite, i.e., the system achieves the global maximum. In the second type,  $\alpha_j = 2$  for all trajectories, with  $\mathbf{x}_j(T) = -\mathbf{x}_j^{\text{tar}}$ , so the Hessian is strictly positive-semidefinite, indicating that the system achieves the global minimum. Finally, the third type of critical points corresponds to  $\alpha_j = 0$  for some trajectories and  $\alpha_j = 2$  for others, i.e., some trajectories achieve their targets but some do not. The Hessian for these critical points is indefinite, indicating a landscape saddle point. We thus conclude that saddle points of the quantum control landscape can arise, unlike the classical scenario in which no saddles appeared for quadratic objective functions. However, no traps are present in either case upon satisfaction of the same three assumptions. We note that the quantum control landscape analogue here, carried out in a unique classically analogous fashion [55], is consistent with prior results as a special reduced case of the unitary matrix control problem [56, 57].

Our analysis above considers only kinematic critical points, at which  $\delta \mathbf{x}_j(T)/\delta \epsilon(t)$  is of

full rank. Singular critical points at which an analogous condition does not hold, however, have been found in quantum scenarios [37, 39, 58]. We expect that they will also exist in the classical landscapes considered in Section III, though we did not encounter any in numerical simulations (Section V). Importantly, singular controls may not necessarily correspond to traps, and may not halt a local gradient algorithm (i.e., the blocking of some local directions on the landscape may still permit successful exploitation of others), but some singular controls may be associated with traps. Singular critical points forming traps have been found to be rare in quantum scenarios, and in light of the formal analogy drawn between the two types of systems here, we expect that they will also be encountered only rarely in classical landscapes [39, 58]. We also add that a reduction of controllability (i.e., Assumption 1) can lead to traps, and significant constraints on control resources (i.e., Assumption 3) can distort the apparent landscape, including with the creation of artificial traps. The impact of the breakdown of any of the three assumptions needs careful further study.

## V. NUMERICAL SIMULATIONS

The results in Section III on the trap-free classical control landscape rest on satisfaction of the second Assumption that  $\delta\mathbf{Z}(T)/\delta\epsilon(t)$  is surjective, which will generally also require satisfaction of Assumptions 1 (controllability) and 3 (free access to control resources). To test the surjectivity assumption, we performed classical optimal control calculations based on Hamilton’s equations for a range of model molecular systems with various Hamiltonians. All simulations start with distinct initial states for the ensemble members and distinguish two types of objectives: “all-to-all” control, in which a different initial state and target is specified for each trajectory in the ensemble, and “all-to-one” control, in which the same target is specified for all trajectories although they start out at distinct initial states. The latter circumstance is considered as a special case, since it is not possible for all trajectories to have exactly the same final state with different initial states, due to the reversibility of classical Hamiltonian dynamics. Thus, the all-to-one simulations become less controllable as the target is more closely approached, so we naturally expect that these cases will be very demanding, resulting in a practical limit on the achieved quality of the control objective and

showing ever higher condition numbers (i.e., ratios of the maximum to minimum singular values) for  $\{\delta\mathbf{Z}(T)/\delta\epsilon(t)\}$  as the target is more closely approached.

The simulations consider the objective function

$$J = - \sum_{i=1}^{\mathcal{M}} \frac{\rho_i}{2} \begin{bmatrix} \mathbf{q}_i(T) - \mathbf{q}_i^{\text{tar}} \\ \mathbf{p}_i(T) - \mathbf{p}_i^{\text{tar}} \end{bmatrix}^T L_i \begin{bmatrix} \mathbf{q}_i(T) - \mathbf{q}_i^{\text{tar}} \\ \mathbf{p}_i(T) - \mathbf{p}_i^{\text{tar}} \end{bmatrix}. \quad (39)$$

where  $\mathbf{q}_i^{\text{tar}}$  and  $\mathbf{p}_i^{\text{tar}}$  are the target positions and momenta, respectively, for the  $i$ th trajectory, and the  $L_i$  are positive-definite matrices. The function in Eq. (39) is the same as that considered in Eq. (16). If the  $(\mathbf{q}_i^{\text{tar}}, \mathbf{p}_i^{\text{tar}})$  are distinct from  $(\mathbf{q}_j^{\text{tar}}, \mathbf{p}_j^{\text{tar}})$  for all values of  $i \neq j$ , then  $J$  enforces all-to-all control, while if the target states are the same for at least some or all of the trajectories,  $J$  attempts to reach all-to-one control as best as possible. In addition, we may partially specify identical target states, e.g., specifying the same target positions  $\mathbf{q}_j^{\text{tar}}$  without specifying the auxiliary target momenta and vice versa. In this case there are in principle an infinite number of accessible auxiliary possible target states, so distinct initial states can all achieve distinct target states while maintaining reversibility of the dynamics. Testing a variety of objective functions allows us to illustrate the theoretical results for a range of scenarios. To this end, we also vary the values of  $L$ ,  $\mathbf{q}^{\text{tar}}$ , and  $\mathbf{p}^{\text{tar}}$  throughout the simulations. The simulations are meant to broadly illustrate the results from the previous sections for a variety of plausible scenarios. We restrict ourselves to relatively simple, low-dimensional systems in order to avoid rising computational costs. We emphasize, however, that the formalism and analysis in Sections II and III is not limited to such simple systems. The tools presented here should enable analogous studies for higher-dimensional systems.

In the following presentation, Section V A will give an overview of the numerical techniques employed. We then present the simulation results, with the cases summarized in Table I and presented in Sections V B–V C. Section V B compares all-to-all and all-to-one control for a two-trajectory ensemble of a model diatomic molecule, while Section V C considers specifying only position targets, only momentum targets, and cases with more than two trajectories. In Sections V B and V C, the molecules in the ensemble are the same, while Section V D presents simulations with distinct molecules. In all simulations, we find that  $\{\delta\mathbf{Z}(T)/\delta\epsilon(t)\}$

Simulation	Subsection	# Variables	Description
1	B	2	All-to-one control
2	B	2	All-to-all control
3	B	2	All-to-all with longer time interval
4	C	2	Position-only control
5	C	2	Momentum-only control
6	C	2-6	All-to-all with more molecules
7	D	6	Simultaneous control of two physical systems (I)
8	D	6	Simultaneous control of two physical systems (II)
9	D	4	Simultaneous control of two physical systems (III)

TABLE I. Simulations presented in Section V.

is surjective to a practical computational level, with a condition number smaller than  $10^5$ . In the all-to-one simulations, we found that the condition number continued to increase as the final state was more closely approached, consistent with the loss of controllability when trying to force initially distinct trajectories to reach a common final point in phase space.

#### A. Numerical techniques: Symplectic integration and D-MORPH optimization algorithms

In the following simulations, unless noted otherwise, the initial control field  $\epsilon_0(t)$  is chosen as a sum of three sine functions with randomly selected amplitudes and phases. The frequencies are taken to be multiples of the fundamental frequency of the system (i.e., found in the absence of a control field). The control field  $\epsilon(t)$  morphed towards its optimal form. The field is discretized on an evenly spaced temporal grid, i.e.,  $t_j = j\Delta t \in [0, T]$ ,  $j = 1, 2, \dots, T/\Delta t$ , where  $\Delta t$  is a small, fixed time-step. During the optimization, the field is allowed to freely vary as a discretized function of time,  $0 \leq t \leq T$ , with the field at each time point treated as a control variable. Finding an optimal control field involves iterating two steps: (i) solving Hamilton’s equations and (ii) updating the control field with the gradient algorithm, until  $J$  has reached a maximum value to acceptable tolerance.

In step (i), a fourth-order symplectic integrator [59] was used to solve Hamilton’s equations (Eq. (6)); a symplectic integrator was chosen for reasons of numerical stability, although

other methods could be utilized. The adopted method involves four substeps to evolve the state from time  $t$  to time  $t + \Delta t$ . Specifically, denoting the state at time  $t$  by  $(\mathbf{q}^0, \mathbf{p}^0)$ , for  $i = 1, 2, 3, 4$ , we have

$$\mathbf{q}^i = \mathbf{q}^{i-1} + b_i \frac{\partial H}{\partial \mathbf{p}}(\mathbf{p}^i) \Delta t, \quad \mathbf{p}^i = \mathbf{p}^{i-1} - c_i \frac{\partial H}{\partial \mathbf{q}}(\mathbf{q}^{i-1}) \Delta t \quad (40)$$

with  $(\mathbf{q}(t + \Delta t), \mathbf{p}(t + \Delta t)) \equiv (\mathbf{q}^4, \mathbf{p}^4)$ . The values of the fixed parameters  $b_i$  and  $c_i$  are given in [60, 61].

In step (ii), the control field is refined using a gradient algorithm based on D-MORPH [62] via a homotopy parameter (progress variable)  $s$ , such that the field is written as  $\epsilon(s, t)$  and  $\epsilon(0, t) = \epsilon_0(t)$ . The D-MORPH equation to update the field is

$$\frac{d\epsilon(s, t)}{ds} \equiv \beta \frac{\delta J}{\delta \epsilon(s, t)}, \quad \beta > 0, \quad (41)$$

ensuring that

$$\frac{dJ}{ds} = \int_0^T \frac{\delta J}{\delta \epsilon(s, t)} \frac{d\epsilon(s, t)}{ds} dt = \beta \int_0^T \left( \frac{\delta J}{\delta \epsilon(s, t)} \right)^2 dt \geq 0. \quad (42)$$

Equation (41) is discretized over time, as described above. The field  $\epsilon(s, t)$  morphs as  $\epsilon(s, t) \rightarrow \epsilon(s + \Delta s, t)$  in order to increase  $J$  until  $\delta J / \delta \epsilon(t) < 10^{-4}$ . Equation (41) is integrated with respect to  $s$  using a fourth-order Runge-Kutta method at each of the time points  $t_j$ . At each increment in  $s$ , the gradient  $\delta J / \delta \epsilon(s, t)$  is computed using Eqs. (15), (18 - 20) once Hamilton's equations are solved and then using Eq. (40) in step (i) based on the control field  $\epsilon(s - \Delta s, t)$  in the preceding iteration.

## B. All-to-one and all-to-all optimal control of a model diatomic molecule

Consider a model vibrating diatomic molecule driven by a control field  $\epsilon(t)$ ,  $t \in [0, T]$ , aligned with the molecular axis. The diatom is modeled as a Morse oscillator with Hamilto-

nian

$$H = \frac{p^2}{2m} + V(q) - D(q)\epsilon(t) = \frac{p^2}{2m} + D_0(1 - e^{-\alpha q})^2 - Aqe^{-\xi q^4}\epsilon(t), \quad (43)$$

where  $q$  and  $p$  are, respectively, the relative distance and momentum between the two atoms. We have removed the center of mass motion and work in internal coordinates; the control landscape in this formulation should still exhibit the general behavior derived in Section III. This Hamiltonian will be used throughout the simulations, except where indicated.

We choose the parameters for the Hamiltonian in Eq. (43) so as to model the internal coordinate motion of the HF molecule, drawing on prior studies [18, 63, 64]. The parameters have the values:  $m = 1732$  (the reduced mass),  $D_0 = 0.2101$  (the dissociation energy),  $\alpha = 1.22$ ,  $A = 0.4541$  and  $\xi = 0.0064$ , all given in atomic units (a.u.). Unless otherwise noted below, the pulse length of the control field is fixed at  $T = 320\pi$  and the initial conditions of the diatom are chosen to be two equally weighted (i.e.,  $\rho_1 = \rho_2 = 0.5$ ) states  $(q_1(0), p_1(0), q_2(0), p_2(0)) = (-0.3, 0, 0, 0.5)$ .

**Simulation 1:** As a reference case, we first simulate the demanding situation of “all-to-one” control by choosing the observable function specified by Eq. (39), with  $q_1^{\text{tar}} = q_2^{\text{tar}} = q^{\text{tar}} = 0.5$  and  $p_1^{\text{tar}} = p_2^{\text{tar}} = p^{\text{tar}} = -5.0$  for *both* trajectories; the matrices in the objective function Eq. (39) are  $L_1 = L_2 = I$ , the identity. The initial control field is chosen to be a sum of three sine functions as described in Section V A; the phases and amplitudes of the sine functions are drawn from a standard normal distribution (0 mean and unit variance) and a uniform distribution over the range  $[0, 0.1]$ , respectively.

The objective function with respect to the progress variable  $s$  is shown in Fig. 1; after a rapid increase, the function value keeps rising, but with ever more difficulty as it attempts to approach  $J = 0$ , as expected from the uncontrollable nature of the objective. Figure 2 shows the initial and final control fields; as commonly found in many quantum control simulations, the final (best) control field shows some resemblance to the initial one. Figure 3 shows that the control field significantly distorts the phase plane trajectories in order to nearly achieve the target, despite the lack of controllability: the final momenta,  $p_1(t)$  and  $p_2(T)$ , reached the target value of  $-5.0$ , but the final positions  $q_1(T) = 0.59$  and  $q_2(T) = 0.41$  differ from the target value of  $0.5$ . Figure 4 shows the condition number of the time-discretized

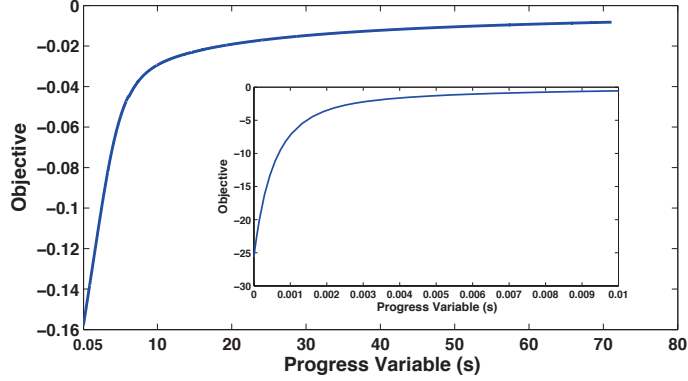


FIG. 1. Objective as a function of the progress variable for an all-to-one target state specification (Simulation 1 in Table I). The inset shows the initial portion of the landscape climb.

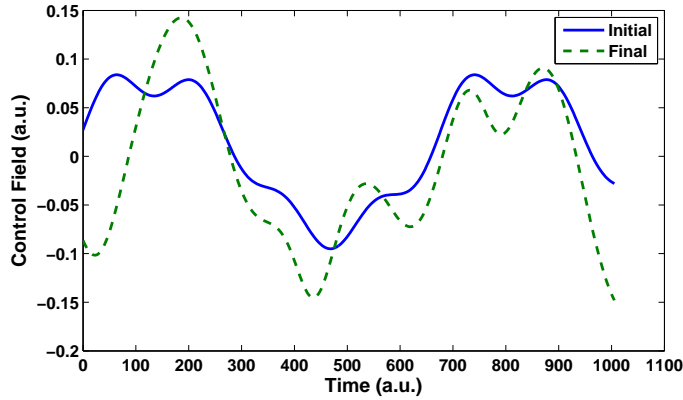


FIG. 2. Initial and final control fields for an all-to-one target state specification (Simulation 1 in Table I).

matrix of  $\delta\mathbf{Z}(T)/\delta\epsilon(t)$  for  $t \in [0, T]$ , where  $\mathbf{Z} = [q_1 \ p_1 \ q_2 \ p_2]^T$ , near the end of the control field evolution. The condition number is modest, near 300, but more importantly continues to increase with  $s$ , which is consistent with an all-to-one objective becoming increasingly singular upon approaching ever closer to the target state.

**Simulation 2:** This case considers the ability to perform all-to-all control. We again consider two trajectories with the same Hamiltonian, initial condition, and final time as in Simulation 1. The objective function is

$$J = -q_1(T)^2 - (p_1(T) - 19.0)^2 - (q_2(T) + 0.2)^2 - (p_2(T) + 5.0)^2, \quad (44)$$

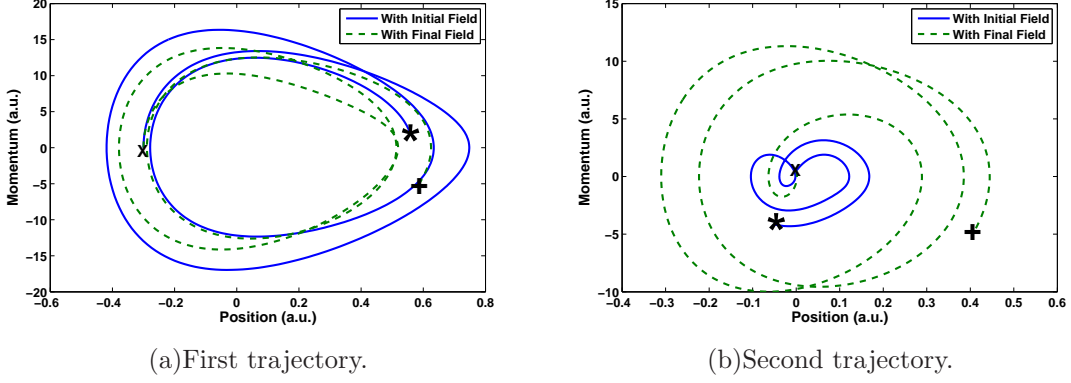


FIG. 3. Individual phase plane trajectories with initial and final control fields for an all-to-one target state specification (Simulation 1 in Table I). The X marks the start of each trajectory; a \* marks the final state of the trajectory with the initial field and a + the final state of the trajectory with the final field. The achieved states with initial and final fields are, respectively,  $(q_1(T), p_1(T), q_2(T), p_2(T)) = (0.57, 2.09, -0.05, -4.16)$  and  $(0.59, -5.00, 0.41, -5.00)$ . The target objective is  $(0.5, -5.0, 0.5, -5.0)$ .

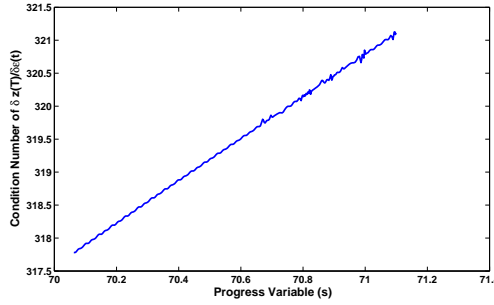


FIG. 4. Condition number of  $\delta \mathbf{z}(T)/\delta \epsilon(t)$  towards the end of the control field iterations for Simulation 1 in Table I.

i.e., Eq. (39) with target states  $(q_1^{\text{tar}}, p_1^{\text{tar}}, q_2^{\text{tar}}, p_2^{\text{tar}}) = (0.0, 19.0, -0.2, -5.0)$ ,  $\rho_1 = \rho_2 = 0.5$ , and  $L_1 = L_2 = 4I$ . We observe a similar evolution in the objective function in Fig. 5a as in Simulation 1 (Fig. 1), with an initial rapid increase followed by a slower approach towards  $J = 0$ . However, unlike the all-to-one case in Simulation 1, the present all-to-all objective should be reachable. The optimal control field (Fig. 5b) significantly distorts the phase plane trajectories (not shown) to achieve final states of  $(q_1(T), p_1(T), q_2(T), p_2(T)) = (0.10, 19.01, -0.20, -5.00)$ , compared to  $(q_1(T), p_1(T), q_2(T), p_2(T)) = (0.31, -11.68, -0.12, 8.31)$  with the initial control field.

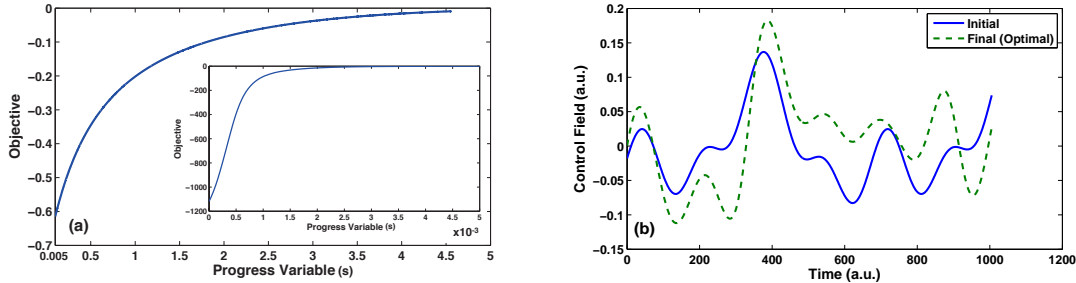


FIG. 5. Simulation results for an all-to-all target state specification (Simulation 2 in Table I). (a) The objective as a function of the progress variable, and (b) the initial and optimal control fields.

The matrix of  $\delta\mathbf{Z}(T)/\delta\epsilon(t)$  has a condition number of 279 at the optimal field, comparable to the all-to-one case. However, unlike the all-to-one simulation, the condition number actually decreases as the near-optimal control field evolves, reflecting the reachability of the all-to-all objective. Similar results were found when different target and initial states were specified.

**Simulation 3:** This case considers an all-to-all objective with a much longer time interval of  $T = 1920\pi$  a.u. to show that subtle changes in the control field can lead to significantly enhancing the final dynamical outcome. These simulations impose the practical condition that the field die away to zero at the beginning and end of the time interval by introducing a Gaussian envelope function  $G(t) = \exp(-81(t - 960\pi)^2 / (1.25 \times 10^7))$  on the control field. Thus, we have  $\epsilon(t) = G(t)E(t)$ , and the field  $\epsilon(t)$  is optimized with respect to the function  $E(t)$ . We choose the initial state to be  $(q_1(0), p_1(0), q_2(0), p_2(0)) = (-0.5, 1.0, 0.5, -1.0)$  and specify the final state as  $(q_1^{\text{tar}}, p_1^{\text{tar}}, q_2^{\text{tar}}, p_2^{\text{tar}}) = (0.8, 10.0, 0.2, 7.0)$ . The objective function in Eq. (39) is chosen have  $\rho_1 = 0.3, \rho_2 = 0.7, L_1 = L_2 = \text{diag}(2, 2 \times 10^{-4})$ .

Figure 6 shows the initial and optimal control fields; the initial function  $E(t)$  is a sum of three sine functions with random amplitudes and phases where the periodicity is chosen to be one half, one, and two times the natural periodicity observed for the field-free system. We see that the changes in the control field are barely perceptible, though the objective function value changes significantly: with the initial control field, the final states are  $(q_1(T), p_1(T), q_2(T), p_2(T)) = (1.12, 5.12, 0.10, 10.05)$ , while with the optimal control field we have  $(q_1(T), p_1(T), q_2(T), p_2(T)) = (0.84, 12.1, 0.21, 7.2)$ . The small change in the control

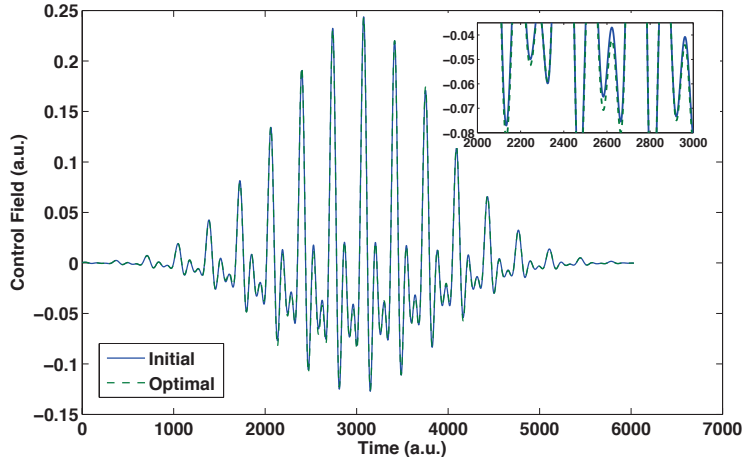


FIG. 6. Initial and optimal control fields for an all-to-all specification with Gaussian envelope having an extended control time interval (Simulation 3 in Table I). The inset magnifies a portion of the fields to reveal their slight difference.

field has an accumulated impact over the extended dynamical time interval, resulting in increased sensitivity of the final state to the control field, as seen by the condition number of  $\delta\mathbf{Z}(T)/\delta\epsilon(t)$  being  $5.76 \times 10^4$  at the optimal control field. From a practical perspective, it is likely best to operate with smaller final times, in keeping with still maintaining control, to permit a measure of significant distinction between the initial and final fields and thereby provide a degree of robustness to small field variations.

### C. Partial target specification and effects of multiple trajectories

This section investigates the control behavior with the Hamiltonian in Eq. (43) when only the momentum or only the position is specified at the target, as well as when more than two trajectories are considered. When optimizing only the position or only the momentum variables, since one of them is free to vary, we expect that sending all position variables to the same value, or all momentum variables to the same value, will be achievable and will not result in singularities (i.e., it is not strictly an example of an all-to-one scenario).

**Simulation 4:** We first examine position target specification for two trajectories, taking the objective function in Eq. (39) to be  $J = -0.5(q_1(T) - 0.8)^2 - 0.5(q_2(T) - 0.8)^2$  with the target position  $q^{\text{tar}} = 0.8$  a.u. for both trajectories. As for Simulation 3 above, we take

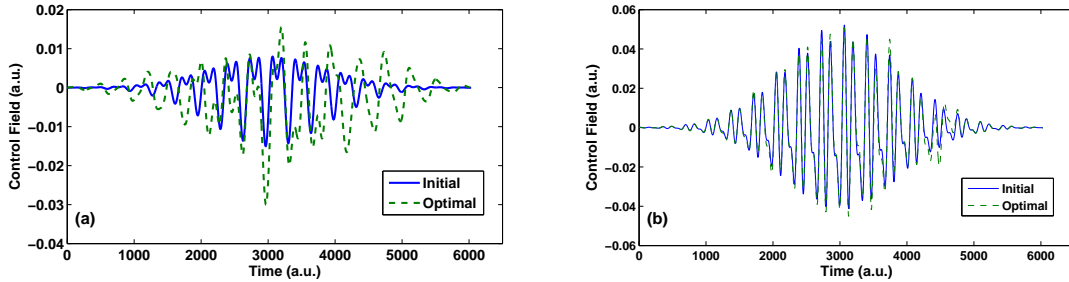


FIG. 7. Initial and final control fields for (a) position- and (b) momentum-only target specification (Simulations 4 and 5 in Table I, respectively).

a large final time of  $T = 1920\pi$  a.u. and multiply the control field by the same Gaussian envelope function  $G(t)$ . The control  $E(t)$  is initialized as the sum of two sine functions with frequencies equal to one and two times the system's fundamental frequency. The initial state variables are  $(q_1(0), p_1(0), q_2(0), p_2(0)) = (-0.5, 1.0, 0.5, -1.0)$ .

Figure 7(a) shows the initial and optimal control fields  $\epsilon(t)$  for this simulation. We see that the overall amplitude of the field is quite low, less than 0.03, compared to the previous cases where all final values of  $\mathbf{q}^{\text{tar}}$  and  $\mathbf{p}^{\text{tar}}$  are specified as goals, posing more stringent demands. The evolution was stopped at  $J = -0.0012$ , with  $(q_1(T), p_1(T), q_2(T), p_2(T)) = (0.800, 16.694, 0.751, 2.251)$ .

**Simulation 5:** This case specifies only the final momenta as the targets  $p_1^{\text{tar}} = p_2^{\text{tar}} = 5.0$  and utilizes the same two initial states and final time as in Simulation 4. Figure 7(b) shows the initial and optimal control fields, which appear very similar, though the optimal control field has a slightly higher amplitude towards the end of the time interval  $[0, T]$ . The final objective function value reached to  $J = -10^{-5}$ , indicating that the target momenta are very closely achieved. The objective function value is thus larger than that obtained when specifying only the position targets in Simulation 4, indicating that it is easier to optimize momentum rather than position targets. This difference is likely due to the fact that the time derivative  $\dot{\mathbf{p}}$  in Eq. (6) is directly coupled to the control field  $\epsilon(t)$  in Eq. (43)'s Hamiltonian, while the evolution  $\dot{\mathbf{q}}$  of the position is coupled to the control field only through the momentum  $\mathbf{p}$ .

**Simulation 6:** To further explore the feasibility of simultaneously controlling a trajectory

Trajectories		$q_1$	$p_1$	$q_2$	$p_2$	$q_3$	$p_3$	$q_4$	$p_4$	$q_5$	$p_5$	$q_6$	$p_6$
2	Initial	-0.5	1.0	0.5	-1.0	-	-	-	-	-	-	-	-
	Target	0.8	10.0	0.2	7.0	-	-	-	-	-	-	-	-
3	Initial	-0.25	1.0	0.25	0	0.75	-1.0	-	-	-	-	-	-
	Target	0.1	-4.8	1.0	2.5	0.5	-4.0	-	-	-	-	-	-
4	Initial	-0.17	1.0	0.17	0.33	0.5	-0.33	0.83	-1.0	-	-	-	-
	Target	0.4	5.1	0	3.7	0.1	12.6	1.1	-10.4	-	-	-	-
5	Initial	-0.125	1.0	0.125	0.5	0.375	0	0.625	-0.5	0.875	-1.0	-	-
	Target	0.3	10.8	0	2.7	0.5	-1.8	0.1	12.3	0.3	23.5	-	-
6	Initial	-0.1	1.0	0.1	0.6	0.3	0.2	0.5	-0.2	0.7	-0.6	0.9	-1.0
	Target	0.2	-7.8	0	2.4	-0.2	-1.0	0.8	5.2	0.1	-14.0	-0.3	-14.4

TABLE II. Initial and target states for ensembles consisting of increasing numbers of multiple trajectories with the Hamiltonian in Eq. (43) for Simulation 6.

ensemble, we again consider all-to-all target specification for the Hamiltonian in Eq. (43), but with consideration of two to six trajectories. In all cases, we use the objective function in Eq. (39) with  $L_i = \text{diag}(1/\mathcal{M}, 1/(100\mathcal{M}))$ . We preferentially weight the momentum due to its larger dynamic range compared to the position. Table II gives the initial and target states  $(q_i(0), p_i(0))$  and  $(q_i^{\text{tar}}, p_i^{\text{tar}})$  for each simulation; the initial states are randomly chosen over the uniform distribution on  $[-1, 1]$ .

As an indication of the difficulty in controlling increasing numbers of trajectories simultaneously, we consider the condition numbers of  $\delta\mathbf{Z}(T)/\delta\epsilon(t)$  for trajectories very near the target objective ( $J < 0.002$ ) and those somewhat further away ( $J \approx 0.1$ ). Figure 8 shows the condition numbers in each case; we see that for both cost function values, the condition numbers first increase and then decrease with the number of trajectories to then finally increase again. Moreover, neither trajectory type yields consistently larger or smaller condition numbers, indicating that the surjectivity of  $\delta\mathbf{Z}(T)/\delta\epsilon(t)$  does not necessarily increase as the final states approach their target values. As the number of trajectories increases, more stringent conditions are placed on the collective controlled evolution, which increases the condition number of  $\delta\mathbf{Z}(T)/\delta\epsilon(t)$ ; however, Fig. 8 shows that these effects are modest.

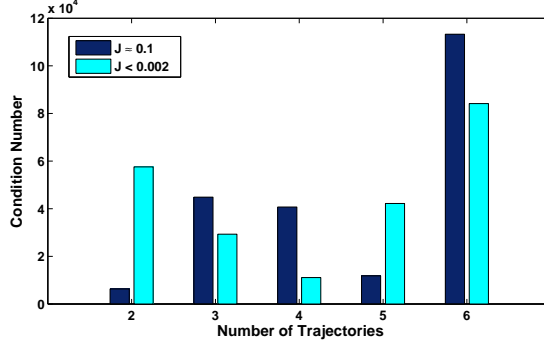


FIG. 8. Condition numbers of  $\delta\mathbf{Z}(T)/\delta\epsilon(t)$  for trajectory ensembles (Simulation 6 in Table I).

#### D. Simultaneous control of two physical systems

This section explores the feasibility of simultaneously controlling two distinct systems with different Hamiltonians, which is of interest in the general scenario of controlling heterogeneous media. The cases will range from those with a pair of very different systems to a pair of very similar systems. Since multiple Hamiltonians introduce additional richness into the ensemble dynamics, we expect that  $\delta\mathbf{Z}(T)/\delta\epsilon(t)$  will remain comfortably surjective.

**Simulation 7:** First, we consider simultaneous control of the one-dimensional Hamiltonian in Eq. (43) along with a two-dimensional system of two coupled Morse oscillators that models the triatomic  $\text{SO}_2$  molecule [65, 66]. We choose a coordinate frame for the latter system in which the two oscillators are coupled through the potential in addition to a kinetic coupling due to the finite mass of the central atom. The dual systems are driven by a single time-dependent control field  $\epsilon(t)$ ,  $t \in [0, T]$ . We let  $(q_2, q_3)$  and  $(p_2, p_3)$  denote the two position and momentum variables, respectively, of the second Hamiltonian:

$$\begin{aligned}
\overline{H}(q_2, p_2, q_3, p_3) &= \frac{1}{2} \left( \frac{p_2^2}{m_2} + \frac{2\beta_k p_2 p_3}{m_2} + \frac{p_3^2}{m_2} \right) + V(q_2, q_3) - D(q_2, q_3)\epsilon(t) \\
&= \frac{p_2^2 + 4\beta_k p_2 p_3 + p_3^2}{2m_2} + d_0 (1 - e^{-\alpha_2 q_2})^2 + d_0 (1 - e^{-\alpha_3 q_3})^2 + \\
&\quad 2d_0\beta (1 - e^{-\alpha_2 q_2}) (1 - e^{-\alpha_3 q_3}) - (q_2 e^{-\xi_0 q_2} - q_3 e^{-\xi_0 q_3}) \epsilon(t). \quad (45)
\end{aligned}$$

The center of mass motion has been removed and the problem is expressed in internal coordinates; as in the single oscillator example, the control landscape in this formulation

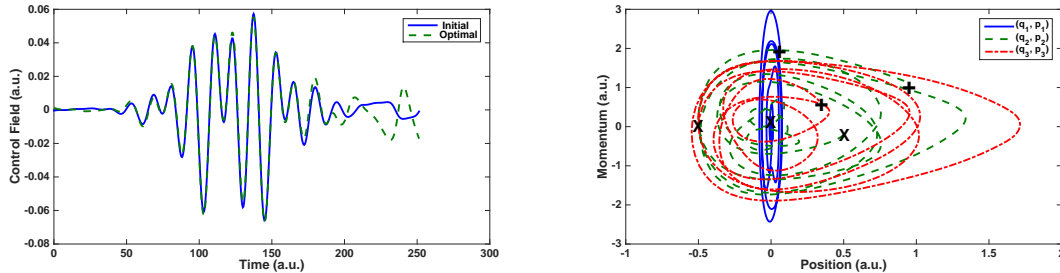


FIG. 9. Simultaneous control over the dynamics with two distinct Hamiltonians (Simulation 7 in Table I). The initial state was  $(q_1(0), p_1(0), q_2(0), p_2(0), q_3(0), p_3(0)) = (0, 0.2, 0.5, -0.2, -0.5, 0)$ , and the final achieved state was  $(q_1(T), p_1(T), q_2(T), p_2(T), q_3(T), p_3(T)) = (0.065, 1.913, 0.954, 1.113, 0.333, 0.654)$  compared to the target of  $(q_1^{\text{tar}}, p_1^{\text{tar}}, q_2^{\text{tar}}, p_2^{\text{tar}}, q_3^{\text{tar}}, p_3^{\text{tar}}) = (0, 1.9, 1.0, 1.0, 0.3, 0.7)$ . The initial and optimal control fields are shown in (a) and the phase space trajectories under optimal control in (b). An 'X' marks the initial states, and the '+' marks the final states.

should still exhibit the general behavior identified in Section III. The parameters in Eq. (45) are chosen to have the values:  $d_0 = 0.2102$ ,  $\alpha_2 = 1.1282$ ,  $\alpha_3 = 0.9712$ ,  $\beta = 0.1$ ,  $\beta_k = -0.1616$ , and  $\xi_0 = 0.1$ ,  $m_2 = 10.667$ , all given in atomic units (a.u.). These parameter values are taken from a model of the  $\text{SO}_2$  molecule used in Ref. [66].

In the subsequent discussion, we use the notation  $\mathbf{Z}(t) = (q_1(t), p_1(t), q_2(t), p_2(t), q_3(t), p_3(t))$  to denote the concatenated state variables; the first coordinates  $(q_1(t), p_1(t))$  correspond to the Hamiltonian in Eq. (43). We choose the initial state to be  $\mathbf{Z}(0) = (0, 0.2, 0.5, -0.2, -0.5, 0)$  and the target state to be  $\mathbf{Z}^{\text{tar}} = (0, 1.9, 1.0, 1.0, 0.3, 0.7)$ . The resulting objective function is given by Eq. (39) with  $L_1 = \text{diag}(2, 0.2)$  and  $L_2 = \text{diag}(2, 2, 0.2, 0.2)$ ,  $\rho_1 = \rho_2 = \rho_3 = 1/3$ . We use a control field pulse length of  $T = 80\pi$  and a Gaussian envelope function  $G(t) = \exp(-(t - 40\pi) \times 10^{-4})$ ; the initial control function  $E(t)$  is a randomly chosen sum of three sine functions as in Simulation 3. To account for the differing periodicities of the two Hamiltonians in Eqs. (43) and (45), we scale the time dynamics of  $(q_1(t), p_1(t))$  by a factor of 8, i.e., we divide the Hamiltonian in Eq. (43) by 8.

Figure 9(a) shows the initial and optimal control fields for Simulation 7. We see that the control field evolves from the initial field, with a particular increase in amplitude near the end of the time interval. The phase space trajectories at the optimal field are shown in Figure 9(b). The two Hamiltonians result in differently shaped trajectories; comparing

$(q_1, p_1)$  to that of  $(q_2, p_2, q_3, p_3)$ , the latter trajectories have a larger range of position and appear aperiodic.

**Simulation 8:** This case considers simultaneous control of a pair of molecules consisting of the system in Eq. (43) along with an altered form of the Hamiltonian in Eq. (45) in order to demonstrate that optimal controls can be found for a variety of dynamical scenarios. In particular, we modify Eq. (45) to be

$$\begin{aligned} \overline{H}(q_2, p_2, q_3, p_3) &= \frac{1}{2} \left( \left( \frac{p_2}{m_2} \right)^2 + \left( \frac{p_3}{m_3} \right)^2 \right) + V(q_2, q_3) - D(q_2, q_3) \epsilon(t) \\ &= \frac{p_2^2}{2m_2} + \frac{p_3^2}{2m_3} + d_0 \left[ (1 - e^{-\alpha_2 q_2})^2 + (1 - e^{-\alpha_3 q_3})^2 + 2\beta (1 - e^{-\alpha_2 q_2}) (1 - e^{-\alpha_3 q_3}) \right] \\ &\quad - (q_2 e^{-\xi_0 q_2} - q_3 e^{-\xi_0 q_3}) \epsilon(t). \end{aligned} \quad (46)$$

This case could arise when the central atom for a triatomic molecule is of very large mass relative to the two end atoms. The parameters in Eq. (46) are chosen to have the values:  $d_0 = 0.2102$ ,  $\alpha_2 = 1.1282$ ,  $\alpha_3 = 0.9712$ ,  $\beta = 0.1$ , and  $\xi_0 = 0.1$ ,  $m_2 = 10.0$ ,  $m_3 = 5.0$ , all given in atomic units (a.u.). We choose the initial state to be  $\mathbf{Z}(0) = (0, 0.2, 0.5 - 0.2, -0.5, 0)$  and the target state to be  $\mathbf{Z}^{\text{tar}} = (0.2, 2.4, 2.0, 0, 0.5, -0.5)$ , with the same objective function, control field pulse length, and Gaussian envelope as in Simulation 7. The initial control function  $E(t)$  is again taken to be a randomly chosen sum of three sine functions, and we again scale the time dynamics of  $(q_1(t), p_1(t))$  by a factor of 8.

Figure 10(a) shows the initial and optimal control fields for Simulation 8, and Fig. 10(b) shows the trajectories of all three  $(q_i, p_i)$  pairs with the final control field. As in Simulation 7, we see that the first  $(q_1, p_1)$  pair has qualitatively different shape from those of the second Hamiltonian, and all of the trajectories are quasi-periodic, in contrast to the aperiodic ones in Figure 9(b).

**Simulation 9:** This scenario addresses another aspect of simultaneous control of multiple systems, relevant to discriminating their presence [67] as has been studied quantum mechanically. We show that Section III's results hold even when two trajectories arising from *near-identical* Hamiltonians are sent to the same target state. We consider the Hamiltonian in Eq. (43) with the Morse potential parameter  $\alpha = 0.97$  for the first

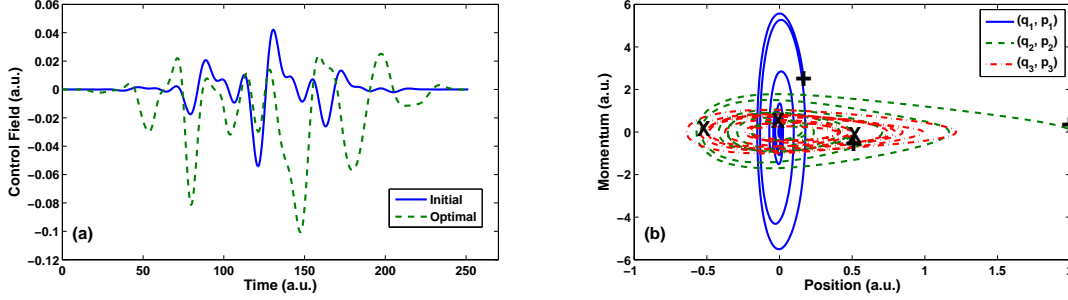


FIG. 10. Simultaneous control over the dynamics with two distinct Hamiltonians (Simulation 7 in Table I). The initial state was  $(q_1(0), p_1(0), q_2(0), p_2(0), q_3(0), p_3(0)) = (0, 0.2, 0.5, -0.2, -0.5, 0)$ , and the final achieved state was  $(q_1(T), p_1(T), q_2(T), p_2(T), q_3(T), p_3(T)) = (0.167, 2.402, 1.983, 0.16, 0.5, -0.524)$  compared to the target of  $(q_1^{\text{tar}}, p_1^{\text{tar}}, q_2^{\text{tar}}, p_2^{\text{tar}}, q_3^{\text{tar}}, p_3^{\text{tar}}) = (0.2, 2.4, 2.0, 0, 0.5, -0.5)$ . The initial and optimal control fields are shown in (a) and the phase space trajectories under optimal control in (b). An 'X' marks the initial states, and the '+' marks the final states.

trajectory  $(q_1, p_1)$  and  $\alpha = 1.22$  for the second trajectory  $(q_2, p_2)$ . The initial state is  $(q_1(0), p_1(0), q_2(0), p_2(0)) = (0, 0.2, 0.5, -0.2)$  and the initial and optimal fields are shown in Figure 11(a); the objective function in Eq. (39) has  $\rho_1 = \rho_2 = 0.5$  and  $L_1 = L_2 = 4I$ . The optimal field is significantly different from the initial field, gaining an additional low-frequency component and increasing in amplitude. The evident high frequency observed in the fields is due to the near, but distinct, frequency structure of the two oscillators. Both trajectories' final states reached the target state of  $(q_1^{\text{tar}}, p_1^{\text{tar}}, q_2^{\text{tar}}, p_2^{\text{tar}}) = (0.2, 2.4, 0.2, 2.4)$  within  $10^{-4}$ , as indicated by the phase space plots in Figure 11(b). Although both trajectories have the same target states, the slight difference in the two Hamiltonians offers just enough dynamical freedom to make the target relatively “easy” to achieve with the condition number of  $\delta\mathbf{z}(T)/\delta\epsilon(t)$  being quite low, at 49.5. Despite the similarity in Hamiltonians, the different initial states cause the trajectories to follow very different paths in the phase space: the first trajectory “spirals out” to reach the target, but the second trajectory spirals in, and the distinctiveness apparently aids in satisfying the surjectivity condition. Interestingly, the time reversal of this control process starting at the point '+' in Figure 11(b) may be interpreted as corresponding to desired discrimination of the two similar systems.

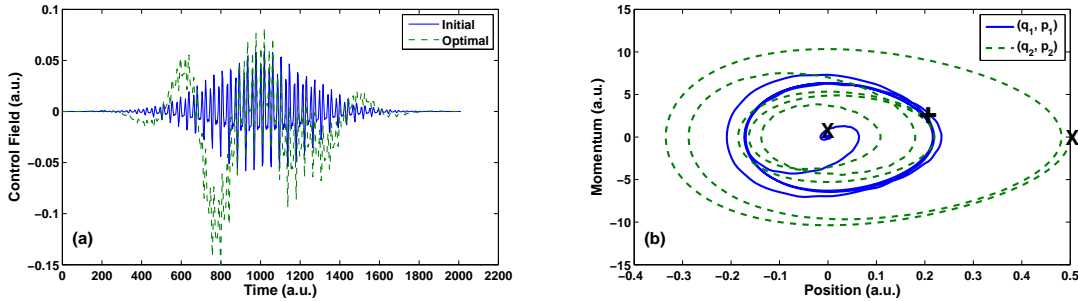


FIG. 11. Results for the ensemble with two similar Hamiltonians (Simulation 8 in Table I). The initial state was  $(q_1(0), p_1(0), q_2(0), p_2(0)) = (0, 0.2, 0.5, -0.2)$ , and the target state was  $(q_1^{\text{tar}}, p_1^{\text{tar}}, q_2^{\text{tar}}, p_2^{\text{tar}}) = (0.2, 2.4, 0.2, 2.4)$ . The initial and optimal control fields are shown in (a) and the phase space trajectories under optimal control in (b). The controlled trajectories achieve their targets within  $10^{-4}$  a.u. An 'X' marks the initial states, and the '+' marks the final states.

## VI. CONCLUSION

This paper examines optimal control landscapes for an ensemble of classical molecular trajectories following Hamiltonian dynamics, focusing in particular on the case of a finite ensemble, e.g., the discretization of an initial distribution in phase space. The objective function aims to send each trajectory of the ensemble to a particular target state in phase space. We derive expressions for the critical points of these control landscapes and use these to determine the Hessian at critical points of the landscape. The Hessian forms a finite-rank matrix, allowing for analysis of conditions under which it is positive- or negative-semidefinite or indefinite. We find that neither saddle critical points nor traps arise on the control landscape, and the finite rank of the Hessian permits finding a bound on the response of  $J[\epsilon(t)]$  to a variation in an optimal control field. The finite rank also implies that a submanifold of optimal control fields exists.

The results in Section III are analogous to the quantum mechanical objective of maximizing the probability that each state in a distinct ensemble of quantum states reaches a specified distinct target. To see this analogy, in Section IV we write the quantum mechanical dynamics in a classical-like framework and compare the resulting critical point and Hessian expressions with their classical counterparts. We find that saddle critical points can arise when only a subset of analogous classical trajectories (respectively quantum states)

reach their targets at the end of the specified time interval. No traps, however, are found: the control landscape has a unique maximum at which all trajectories (resp. states) reach their targets. The similarity between the classical and quantum landscapes extends to the landscape Hessian: the Hessians in both circumstances have finite rank, permitting their expression in terms of a finite linear combination of orthogonal, linear independent functions. However, the quantum analogue has saddles arising from the extra condition on the normalization of each state, while the classical case has no such extra condition on its states and therefore no saddles are present. The latter conclusion is also consistent with the simulations, where *none* of the plots of  $J(s)$  have indicated the characteristic behavior of slowing down upon coming close to a saddle.

The analysis in Section III rests on the nature of the objective functional, the controllability and surjectivity of the system, and access to any desired control. As in the quantum case, it would be interesting to investigate the fundamental and practical consequences of violating the assumptions to varying degrees. Moreover, further examination of the continuous classical ensemble control in Section III A would be interesting, particularly considering the subtle issues of controllability and surjectivity. Additional applications of the present work may also extend to control of classical systems in engineering contexts, e.g., [26–29], including to the synchronization of multiple coupled oscillators [68–71].

## ACKNOWLEDGEMENTS

We gratefully acknowledge useful discussions with Ruixing Long.

C.J.-W. acknowledges support from the Princeton Program in Plasma Science and Technology and NDSEG Fellowship. H. R. acknowledges partial support from the ARO (#W911NF-13-1-0237) and ARO-MURI (#W911NF-11-1-2068), while T.-S. H. acknowledges partial support from the DOE (#DE-FG02-02ER15344) and NSF (#CHE-1058644). R.-B. W. acknowledges support from NSFC Grants No. 61374091 and No. 61134008.

---

[1] C. Brif, R. Chakrabarti, and H. Rabitz, *New Journal of Physics*, **12**, 075008 (2010).

- [2] H. Rabitz, R. de Vivie-Riedle, M. Motzkus, and K. Kompa, *Science*, **288**, 824 (2000).
- [3] W. S. Warren, H. Rabitz, and M. Dahleh, *Science*, **259**, 1581 (1993), ISSN 0036-8075.
- [4] M. E. Tuckerman and G. J. Martyna, *The Journal of Physical Chemistry B*, **104**, 159 (2000).
- [5] T. D. Sewell and D. L. Thompson, *International Journal of Modern Physics B*, **11**, 1067 (1997).
- [6] G. H. Peslherbe, H. Wang, and W. L. Hase, *Advances in Chemical Physics: Monte Carlo Methods in Chemical Physics*, Volume 105, 171 (2007).
- [7] M. Karplus and J. A. McCammon, *Nature Structural & Molecular Biology*, **9**, 646 (2002).
- [8] E. F. de Lima and M. A. M. de Aguiar, *Physical Review A*, **77**, 33406 (2008), ISSN 1094-1622.
- [9] R. B. Gerber, M. V. Korolkov, J. Manz, M. Y. Niv, and B. Schmidt, *Chemical Physics Letters*, **327**, 76 (2000), ISSN 0009-2614.
- [10] S. Kreml, T. Eisenhammer, A. Hübler, G. Mayer-Kress, and P. W. Milonni, *Physical Review Letters*, **69**, 430 (1992).
- [11] C. D. Schwieters and H. Rabitz, *Physical Review A*, **44**, 5224 (1991).
- [12] C. D. Schwieters and H. Rabitz, *Physical Review A*, **48**, 2549 (1993).
- [13] R. B. Walker and R. K. Preston, *The Journal of Chemical Physics*, **67**, 2017 (1977).
- [14] V. S. Batista and P. Brumer, *Physical Review Letters*, **89**, 143201 (2002), ISSN 1079-7114.
- [15] J. Botina, H. Rabitz, and N. Rahman, *The Journal of Chemical Physics*, **102**, 226 (1995).
- [16] J. Botina, H. Rabitz, and N. Rahman, *Physical Review A*, **51**, 923 (1995), ISSN 1094-1622.
- [17] M. Demiralp and H. Rabitz, *Journal of Mathematical Chemistry*, **16**, 185 (1994).
- [18] A. Efimov, A. Fradkov, and A. Krivtsov, in *Proceedings of the European Control Conference Cambridge, UK* (2003) pp. 1–4.
- [19] V. Engel, C. Meier, and D. Tannor, in *Advances in Chemical Physics*, *Advances in Chemical Physics*, Vol. 141, edited by S. Rice (John Wiley & Sons, 2009) ISBN 9780470417133.
- [20] J. L. Krause, R. M. Whitnell, K. R. Wilson, and Y. J. Yan, in *AIP Conference Proceedings*, Vol. 298 (Citeseer, 1993) pp. 3–15.
- [21] M. H. Lissak, J. D. Sensabaugh, C. D. Schwieters, J. G. B. Beumee, and H. Rabitz, *The Journal of Chemical Physics*, **174**, 1 (1993).
- [22] Y. Nishiyama, T. Kato, Y. Ohtsuki, and Y. Fujimura, *The Journal of Chemical Physics*, **121**, 2685 (2004).

- [23] H. Umeda and Y. Fujimura, *The Journal of Chemical Physics*, **113**, 3510 (2000).
- [24] Y. J. Yan, R. E. Gillilan, R. M. Whitnell, K. R. Wilson, and S. Mukamel, *The Journal of Physical Chemistry*, **97**, 2320 (1993), ISSN 0022-3654.
- [25] C. Joe-Wong, T.-S. Ho, R. Long, H. Rabitz, and R. Wu, *The Journal of Chemical Physics*, **138**, 124114 (2013).
- [26] N. Chopra and M. W. Spong, *Automatic Control, IEEE Transactions on*, **54**, 353 (2009).
- [27] F. Dörfler and F. Bullo, *Automatica* (2014).
- [28] D. S. Goldobin, *The European Physical Journal Special Topics*, **223**, 677 (2014).
- [29] A. E. Hramov, A. A. Koronovskii, and O. I. Moskalenko, *Physics Letters A*, **354**, 423 (2006).
- [30] T.-S. Ho and H. Rabitz, *Journal of Photochemistry and Photobiology A: Chemistry*, **180**, 226 (2006), ISSN 1010-6030.
- [31] M. Hsieh, R. Wu, and H. Rabitz, *The Journal of Chemical Physics*, **130**, 104109 (2009).
- [32] H. Rabitz, T.-S. Ho, M. Hsieh, R. Kosut, and M. Demiralp, *Physical Review A*, **74**, 12721 (2006).
- [33] H. Rabitz, M. Hsieh, and C. Rosenthal, *Science*, **303**, 1998 (2004).
- [34] R. Wu, H. Rabitz, and M. Hsieh, *Journal of Physics A: Mathematical and Theoretical*, **41**, 015006 (2008).
- [35] J. Roslund and H. Rabitz, *Physical Review Letters*, **112**, 143001 (2014).
- [36] Q. Sun, I. Pelczer, G. Riviello, R.-B. Wu, and H. Rabitz, *Physical Review A*, **89**, 033413 (2014).
- [37] R.-B. Wu, M. A. Hsieh, and H. Rabitz, *Physical Review A*, **83**, 062306 (2011).
- [38] K. W. Moore and H. Rabitz, *The Journal of chemical physics*, **137**, 134113 (2012).
- [39] R.-B. Wu, R. Long, J. Dominy, T.-S. Ho, and H. Rabitz, *Physical Review A*, **86**, 013405 (2012).
- [40] A. Pechen and H. Rabitz, *Europhysics Letters*, **91**, 60005 (2010).
- [41] C. M. Tesch and R. de Vivie-Riedle, *Physical Review Letters*, **89**, 157901 (2002).
- [42] P. von den Hoff, S. Thallmair, M. Kowalewski, R. Siemering, and R. de Vivie-Riedle, *Physical Chemistry Chemical Physics*, **14**, 14460 (2012).
- [43] R. D. Taylor and P. Brumer, *The Journal of Chemical Physics*, **77**, 854 (1982).

- [44] C. Cai, Z. Xu, and W. Xu, *Automatica*, **38**, 1927 (2002).
- [45] Y. Lai, M. Ding, and C. Grebogi, *Physical Review E*, **47**, 86 (1993).
- [46] E. Ott, C. Grebogi, and J. Yorke, *Physical review letters*, **64**, 1196 (1990).
- [47] Z. Wu, Z. Zhu, and C. Zhang, *Physical Review E*, **57**, 366 (1998).
- [48] E. D. Sontag, *Mathematical Control Theory: Deterministic Finite Dimensional Systems*, Texts in applied mathematics (Springer, 1998) ISBN 9780387984896.
- [49] B. Bonnard and M. Chyba, *Singular Trajectories and Their Role in Control Theory* (Springer Verlag, 2003).
- [50] R. W. Brockett, *Finite Dimensional Linear Systems*, Series in decision and control (Wiley, 1970).
- [51] A. J. Dragt, *Annals of the New York Academy of Sciences*, **1045**, 291 (2005).
- [52] G. Riviere, C. Brif, R. Long, R.-B. Wu, K. M. Tibbetts, T.-S. Ho, and H. Rabitz, arXiv preprint arXiv:1405.0204 (2014).
- [53] H. Rabitz, M. Hsieh, and C. Rosenthal, *The Journal of Chemical Physics*, **124**, 204107 (2006).
- [54] K. Hoffman and R. A. Kunze, *Linear Algebra*, Prentice-Hall mathematics series (Prentice-Hall, 1971).
- [55] F. Strocchi, *Reviews of Modern Physics*, **38**, 36 (1966).
- [56] M. Hsieh and H. Rabitz, *Physical Review A*, **77**, 042306 (2008).
- [57] T.-S. Ho, J. Dominy, and H. Rabitz, *Physical Review A*, **79**, 013422 (2009).
- [58] R. Wu, J. Dominy, T.-S. Ho, and H. Rabitz, Arxiv preprint (2009), arXiv:0907.2354.
- [59] J. Candy and W. Rozmus, *Journal of Computational Physics*, **92**, 230 (1991), ISSN 0021-9991.
- [60] D. Donnelly and E. Rogers, *American Journal of Physics*, **73**, 938 (2005).
- [61] R. I. McLachlan and P. Atela, *Nonlinearity*, **5**, 541 (1992).
- [62] A. Rothman, T.-S. Ho, and H. Rabitz, *The Journal of Chemical Physics*, **123**, 134104 (2005).
- [63] A. Guldberg and G. D. Billing, *Chemical Physics Letters*, **186**, 229 (1991), ISSN 0009-2614.
- [64] J. R. Stine and D. W. Noid, *Optics Communications*, **31**, 161 (1979), ISSN 0030-4018.
- [65] M. L. Sage and J. A. Williams III, *The Journal of Chemical Physics*, **78**, 1348 (1983).
- [66] M. D. Radicioni, C. G. Diaz, and F. M. Fernandez, *Journal of Molecular Structure (Theochem)*, **488**, 37 (1999).

- [67] B. Li, G. Turinici, V. Ramakrishna, and H. Rabitz, *The Journal of Physical Chemistry B*, **106**, 8125 (2002).
- [68] D. A. Paley, N. E. Leonard, R. Sepulchre, D. Grunbaum, and J. K. Parrish, *Control Systems, IEEE*, **27**, 89 (2007).
- [69] S.-J. Chung and J.-J. Slotine, *Robotics, IEEE Transactions on*, **25**, 686 (2009).
- [70] F. Dörfler, M. Chertkov, and F. Bullo, *Proceedings of the National Academy of Sciences*, **110**, 2005 (2013).
- [71] L. F. R. Turci and E. E. Macau, *Chaos: An Interdisciplinary Journal of Nonlinear Science*, **22**, 033151 (2012).